

The image is a satellite photograph of Antarctica, showing the continent's ice sheets and various meltwater features. A solid blue horizontal band is overlaid at the top, containing the title and subtitle in white text. The rest of the image shows the intricate patterns of ice and meltwater on the Nivlisen ice shelf.

Analysing the development of meltwater networks on Antarctica

A casestudy on the Nivlisen ice shelf

Geerten van der Zalm

Analysing the development of meltwater networks on Antarctica

A case study on the Nivlisen ice shelf

by

G.W.E. van der Zalm

to obtain the degree of Master of Science
at Delft University of Technology,
to be defended publicly on Thursday September 3, 2020 at 14:00.

Student number: 4232224
Thesis committee: Dr. T. A. Bogaard, TU Delft, supervisor
Dr. S. L. M. Lhermitte, TU Delft
Dr. Ir. M. Hrachowitz, TU Delft

An electronic version of this thesis is available at <http://repository.tudelft.nl/>.

Cover image: Landsat 8 imagery, image courtesy of the U.S. Geological Survey

Preface

This thesis analyses observed meltwater networks in Antarctica during the summer of 2016-2017. Working on this research was challenging and I hope to be able to look back at this period happily and with pride.

I would like to thank my committee members for their supervision. I remember being fascinated by the satellite imagery of and videos made on Antarctica that Stef Lhermitte showed me during our first meeting, which definitely sparked my interest in this topic. During my thesis, his expertise on the relevant processes and his suggestions to further improve my work were very helpful. Especially the time he spent on helping me with a difficult reprojection of the climate data was really appreciated. Thom Bogaard helped me see the next possible steps during my thesis and the value of the research. During more difficult times he was always available for shorter or longer talks and Skype sessions when needed. His practical advice on writing and the frequent meetings we had, have definitely helped me to improve the quality of this thesis a lot. Thanks a lot Thom! Markus Hrachowitz could always contribute with a lively brainstorm where new ideas were excitedly discussed, entirely in the style of his interesting and inspiring lectures on hydrological modelling. His life lesson to never take the average over an area when making a hydrological model was definitely applied in this thesis.

A special thanks goes to Rebecca Dell, who is frequently cited in this thesis. She responded very enthusiastically to my emails and was happy to share her data with me. In this way, she made me feel part of a larger community of scientists and gave me extra motivation to work on my research.

Furthermore, I would like to thank all my fellow graduate students who I worked alongside during my time in the different rooms at the fourth floor. I met a lot of great people, who always provided some (much needed) distractions and fun times during our hard labour. Without the printed quotes, art works, photoshopped posters, music, lunches, dinners, walks and Christmas drinks, I would have never made it to this point. Lastly, a big thanks goes to Lydia and Betty, who were able to tolerate the crazy stuff we sometimes did as students, provided us with large computer monitors and sweets and made the fourth floor a welcoming place to be.

*Geerten van der Zalm
Delft, September 2020*

Summary

This thesis presents an analysis of the meltwater features that developed on the Nivlisen ice shelf in Antarctica during the melting season of 2016-2017. Meltwater features are present on ice shelves all around Antarctica. These meltwater features could either destabilize ice shelves by exerting additional loading forces, or prevent destabilization by exporting meltwater from the ice shelf into the ocean. The ice shelves play an important role in controlling the discharge of land ice from the Antarctic continent into the ocean by providing a resisting force against this ice flow. Therefore, the rate of global mean sea level rise depends on the future of the Antarctic ice shelves. The development of surface meltwater networks is a process not fully understood. In this thesis three aspects are studied. 1) The development of meltwater features during one melting season, 2) the influence of topography on the shape and extent of a meltwater network, and 3) the link between climate data and the observed developments of the meltwater features.

Three data sources have been combined in this study. First of all, optical satellite imagery was used to track the development of meltwater features during one melting season. The area, depth and volume of the meltwater features were calculated using the Reference Elevation Model of Antarctica. Second, the same elevation model was used as input for running a routing algorithm to create a potential routing network. With the routing network the influence of topography on the shape of meltwater networks was researched. A workflow was proposed to ensure that depressions were handled correctly. Finally, climate data from RACMO was analysed. Meltwater and refreezing data were combined to study the modelled nett meltwater production. The modelled nett meltwater production was compared to the changes in the calculated volumes of observed meltwater features.

The calculated depth, volume and area of the meltwater features were in line with a study by Dell et al. (2020). Both volume and area showed clear trends over the melting season, steadily growing at first and declining when the peak of the summer was over. The first meltwater features developed close to the grounding line. Later in the season, these individual features connected and formed a network which extended seawards until halfway between the grounding line and the ice shelf cliff. The depth of meltwater features was fairly constant over time. The accuracy of the potential routing networks is strongly dependent on the correct use of a depression depth threshold. The deepest depressions on an ice shelf have to be included as endpoints for the routing algorithm to obtain realistic results. The created potential routing networks for the Nivlisen ice shelf matched the observed meltwater features very well. The modelled meltwater production and refreezing turned out to be very similar. Modelled meltwater was for the major part of the summer immediately refrozen, resulting in a nett meltwater production close to zero. Since observations show that meltwater is present on the ice shelf, climate data underestimates the meltwater production significantly. Additionally, distinct regions were identified with a high number of days of positive modelled nett meltwater production. These regions coincided with the regions where meltwater features were observed.

During the melting season, meltwater features started out as individual lakes. Later on, channels connected these lakes and started forming a network which evolved seaward. The shape, extent and calculated dimensions matched the analyses found in other studies. Topography is the determining factor for the shape of meltwater networks on the Nivlisen ice shelf. Depressions served as endpoints for the developing meltwater networks and possibly prevent a network to extend to the ocean. The developed routing method works well and can be applied on other ice shelves as well. Modelled climate data underestimated the meltwater production rate or overestimated the refreezing rate. Therefore the climate data could not be used to explain the development of meltwater features. However, it does provide a first indication of locations where meltwater features can develop.

This thesis contributed to the understanding of processes related to meltwater development on an Antarctic ice shelf. It is advised that future research focusses on the representation of hydrological processes in climate models to improve the estimations of meltwater production and refreezing rate.

Contents

List of Figures	vi
List of Tables	vi
1 Introduction	1
1.1 Background	1
1.2 Antarctic processes	2
1.3 Problem statement	3
1.4 Theoretical framework	3
1.4.1 Seasonal development of meltwater networks	4
1.4.2 Topography and routing	4
1.4.3 Climate data	5
2 Method	7
2.1 Study area	7
2.2 Observations	8
2.2.1 Satellite data	8
2.2.2 Digitization	8
2.2.3 Depth and volume calculations	8
2.2.4 Comparison to Dell (2020)	9
2.3 Routing	9
2.4 Climate data	11
3 Results and Discussion	12
3.1 Meltwater observation	12
3.1.1 Area	12
3.1.2 Depth and volume	12
3.1.3 Comparison to Dell et al. (2020)	13
3.1.4 Discussion	13
3.2 Topography and routing	16
3.2.1 Routing algorithm	16
3.2.2 Influence of depressions	16
3.2.3 Discussion	17
3.3 Climate data / physical drivers	18
3.3.1 Correlation	19
3.3.2 Meltwater production: development during season	20
3.3.3 Daily melt and refreeze	21
3.3.4 Discussion	21
3.4 Roi Baudouin ice shelf	22
3.4.1 Area and volume	23
3.4.2 Topography and routing	23
3.4.3 Climate data	23
3.4.4 Discussion	24
3.5 General discussion	24
3.5.1 Calculated volumes in relation with RACMO climate data	25
3.5.2 Future development of the meltwater network	26
3.5.3 Role of firm air content	27
3.5.4 Influence of climate change	27

4	Conclusions and recommendations	28
4.1	Conclusions.	28
4.2	Recommendations	29
4.2.1	Closing the water balance	29
4.2.2	RACMO constrained by observed meltwater volume.	29
4.2.3	Study firm air content	29
4.2.4	Routing on multiple ice shelves	29
4.2.5	Radar satellites.	29
	Bibliography	31
A	Appendix A	35
A.1	Glossary.	35
A.2	Datasets.	35
A.3	Additional figures.	36

List of Figures

1.1	Explanation of Antarctic processes	2
2.1	Overview of the study area	7
2.2	Flow diagram for depth and volume calculations	8
2.3	Illustration of depth calculations	9
2.4	Flow diagram for the routing method	10
3.1	The maximum meltwater extent during the melting season	13
3.2	Meltwater area, depth and volume calculations	14
3.3	The progression of the meltwater front	15
3.4	The potential routing network	17
3.5	The potential routing networks created without accurate thresholds	18
3.6	Radiation and temperature during the melting season	19
3.7	Pearson correlation for radiation and temperature	19
3.8	Modelled snowmelt, refreezing and nett melt production	20
3.9	Spatial pattern of temporal mean modelled snowmelt and refreeze data	21
3.10	Daily climate data	22
3.11	Spatial pattern of positive nett meltwater production	23
3.12	Potential routing networks on the Roi Baudouin ice shelf	24
3.13	Daily climate data for the Roi Baudouin ice shelf	25
3.14	Spatial pattern of mean snowmelt and refreeze data on the Roi Baudouin ice shelf	26
3.15	Spatial pattern of nett positive melt days on the Roi Baudouin ice shelf	26
3.16	Meltwater networks until 2020	27
A.1	Extent of meltwater features for all time steps	36
A.2	Graphic overview of the routing method	37

List of Tables

1.1	GMSL rise in three RCP scenarios	1
2.1	List of dates used in this study	8
A.1	Datasets used	35

Introduction

1.1. Background

The thick land based ice sheet¹ of Antarctica holds up to 60 metres worth of global mean sea level (GMSL) rise. Current climate projections indicate that the estimated contributed GMSL rise of the Antarctic ice sheet for 2100 is limited to 0.06 metre under Representative Concentration Pathway (RCP) 4.5 (Table 1.1)(Oppenheimer et al., 2019).

Table 1.1: The three main RCP scenarios and their respective GMSL rise contribution on Antarctica and the total GMSL rise for 2100 (Oppenheimer et al., 2019).

RCP scenarios and GMSL rise, 2100		
scenario	Antarctica [m] median(95% interval)	Total [m] median(95% interval)
RCP 2.6	0.04(0.01-0.11)	0.43(0.29-0.59)
RCP 4.5	0.06(0.01-0.15)	0.55(0.39-0.72)
RCP 8.5	0.12(0.03-0.28)	0.84(0.61-1.10)

The relative contribution of Antarctica to GMSL rise increases when extending the projections beyond the year 2100. On these long time scales, the Antarctic and Greenland ice sheet contribute the most to GMSL rise. The total GMSL rise and its timing may be strongly dependent on two tipping points, a sudden and irreversible effect caused by a gradual change. One tipping point addresses the retreat of the Greenland ice mass. The other is about the possible decrease in stability of the Antarctic ice shelves* (Deconto and Pollard, 2016). The timing of these tipping points, which are expected to be strongly dependent on the different climate scenarios the world could follow, is very uncertain (Meredith et al., 2019).

The exact future behaviour of the Antarctic ice sheet is difficult to predict. Ice flow may accelerate dependent on changes in the forces acting on the ice sheet. The ice shelves, floating ice connected to the Antarctic mainland, provide one of these forces. It is a resisting force against the ice flow, called the buttressing effect (Rignot et al., 2013). This force limits the ice discharge from the upstream ice sheet and is provided by friction between the ice shelf and the sea bed and side walls (Goldberg, 2017). A possible break up of the ice shelves would reduce the buttressing effect. As a result the discharge of land ice into the ocean would increase, causing the GMSL rise to accelerate (Reese et al. (2018), Fürst et al. (2016) and Dupont and Alley (2005)). The exact mechanism behind the break up of ice shelves is not fully understood (Bell et al., 2018). It is argued that the fast disintegration of the Larsen B ice shelf, a large ice shelf on the Antarctic Peninsula (Figure 2.1), was triggered by the rapid drainage of the surface lakes present on the shelf and the subsequent crack development throughout the ice shelf (Banwell et al., 2013). Water concentrating on one place, forming a lake, provides an additional loading on the ice shelf, flexing the shelf downwards. After draining of the lake through (small) cracks, the ice shelf flexes upwards again. This cycle can destabilize the ice shelf (Banwell and MacAyeal, 2015). Moreover, when water refreezes in a crack, it expands and thus increases the size of the crack (Scambos et al., 2000). These two processes lead to a decreased stability of the ice shelf and could break it up (Banwell et al., 2013). There are indications that the melt intensities on multiple ice shelves will

¹The definition of some words used in this report are given in Appendix A.1 and are indicated from now on with a *.

pass the melt rate prior to the break up of the Larsen B ice shelf by 2100. This is especially the case under RCP 8.5 and mainly on the Antarctic Peninsula (Trusel et al., 2015). However, there is a possibility that increased melting rates do not necessarily lead to break up events, if water is not ponded on the ice shelf surface, but instead transported towards the ocean (Bell et al., 2017). Observations of extensive surface water networks, extending up to 120 kilometres (Kingslake et al., 2017a), could indicate that ice shelves are indeed able to discharge meltwater into the ocean and thus mitigate the destabilizing effect of ponded meltwater (Bell et al., 2017). However, little is known about the processes determining the fate of surface water on the Antarctic ice shelves.

In this research, an analysis of a meltwater drainage network on an Antarctic ice shelf is presented. It will focus on the potential shape of a drainage network and the evolution of such a network during one melting season.

Before continuing to the problem statement and the questions posed in this study, a short introduction into general Antarctic processes is given. This will focus on the surface mass balance (SMB) processes, which are important for GMSL rise. This introduction was written to help laymen better understand the processes mentioned in this study and grasp the relations between this study and the larger framework of climate change research.*

1.2. Antarctic processes

In contrast to the North Pole, the majority of the ice of Antarctica does not float, but rests upon bedrock (figure 1.1.a). A thick layer of ice, over 3 kilometres thick at some places, covers this bedrock (Fretwell et al., 2013). The thick ice layer becomes thinner towards the edges of the Antarctic continent and due to the weight of the ice sheet, ice slowly flows from the centre outwards. At a certain point towards the edge of the continent, ice will start to float while still attached to the ice on the bedrock. The line where ice starts to float is called the grounding line* (Figure 1.1.b). These floating parts are called ice shelves. They can be found along 75% of the coasts of Antarctica (Rignot et al., 2013). Ice shelves provide a resisting force against the flow of ice from the continent, called a buttressing effect (Fürst et al., 2016). Due to various natural processes, ice breaks off from ice shelves and becomes an iceberg. Due to the constant flow of ice from the mainland onto the ocean, ice shelves grow again over time after a break of event. The lost ice mass by the breaking off of icebergs is compensated by snowfall on the mainland. In a stable system, there is a balance between the mass loss (losing of icebergs and additionally melt of ice) and the mass gain (snowfall). However, ice shelves are losing mass more quickly the past decades (Paolo et al., 2015) and large break up events have been recorded (Banwell et al., 2013). This decreases the resisting force that the ice shelves provide (Dupont and Alley, 2005). Therefore, the flow of ice from the mainland is accelerating (Reese et al., 2018). Antarctica is thus no longer in balance: more mass is lost than gained. As a result, more water is present in the worlds oceans and the global mean sea level rises.

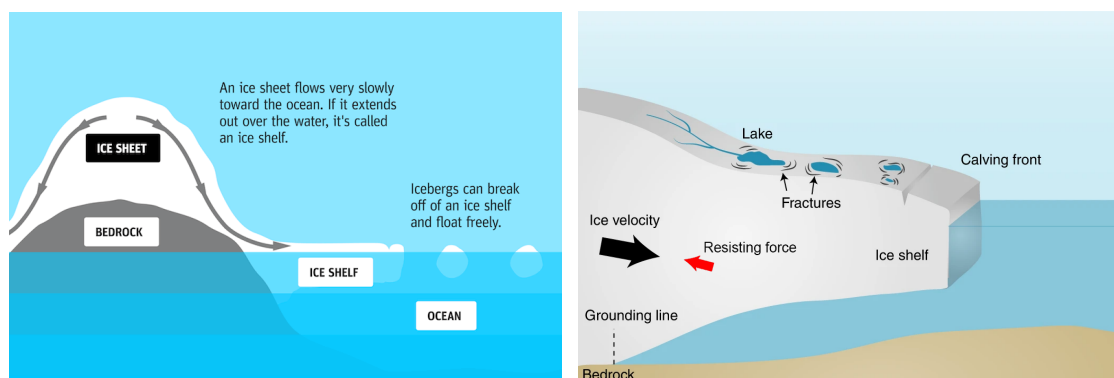


Figure 1.1: a) A simplification of Antarctica. A thick ice sheet rests upon a bedrock layer and slowly discharges ice from the mainland into the ocean. b) A visualization of one ice shelf. Ice is no longer in contact with the bedrock layer, but floats on the ocean. Meltwater collects in streams and lakes, possibly causing fractures in the ice shelf. This weakens the ice shelf and makes it more prone to a breakup event.

As mentioned, the break up of ice shelves is a natural process. But likely due to an increase in temperature (Scambos et al., 2000), this process is accelerated. One process that was recently observed and is argued to be a cause for ice shelf break up, is the ponding of meltwater (Banwell et al., 2013). When ice at the surface melts, the water can infiltrate into the ice/snow layer. It is also possible that water flows over the surface and collects in streams and lakes (figure 1.1.b). The concentration of water on one place, adds an extra force. This has the potential to weaken the ice shelf by creating fractures (Banwell and MacAyeal, 2015). Consequently, new water can fill these cracks, and could make the cracks bigger (Scambos et al., 2000). Once multiple cracks are present and propagate through the entire thickness of the ice shelf, a break up event can occur (Banwell et al., 2013). Recently it was argued, that the concentration of meltwater in streams could be able to also prevent break up events. Streams could bring the water towards the edge of the ice shelf and discharge it directly into the ocean (Bell et al., 2017). In this way, water does not stay on the ice shelf in lakes and thus no additional loading is present. So far, the understanding of these meltwater streams is limited (Bell et al., 2018).

In the next section, the problem statement is summarized. Afterwards, the three questions that this thesis tried to answer are given.

1.3. Problem statement

Destabilization of ice shelves reduces the resisting force against ice flow from the grounded part of Antarctica into the ocean. This results in an acceleration of the ice flow. Surface meltwater networks are thought to have an important role in the mechanisms influencing the ice shelf stability. They could decrease the stability by creating additional loading forces when meltwater ponds, but they could also help to prevent this destabilization of the ice shelf by exporting meltwater towards the ocean. Knowledge is lacking on the processes of the creation and evolution of meltwater networks. Therefore this thesis will try to answer the following questions:

1. What is the temporal and spatial development of meltwater networks during one melting season?
2. Is the topography of an ice shelf a driver for the shape and extent of a meltwater network?
3. Is it possible to identify underlying physical drivers of the creation of meltwater networks using available climate data?

The next section contains a theoretical framework for each question posed above. It describes previous research and forms a basis for the methods described in section 2. But first, a broader background is given containing information about GMSL rise and the processes related to ice shelf breakup.

1.4. Theoretical framework

Table 1.1 showed the projected GMSL rise for the three main RCP scenarios developed in the IPCC report published in 2019 (Oppenheimer et al., 2019). However, recent research introduced both a larger and more uncertain contribution to the GMSL rise from Antarctica (Deconto and Pollard, 2016). They included an additional process for ice shelf break up in GMSL rise models. Sea levels during interglacial periods were better represented in this way. Consequently, these models were applied to the RCP climate scenarios. This created possible envelopes for the Antarctic contribution to GMSL rise up until the year 7000. Only under RCP2.6 was the contribution limited, but for RCP8.5 the Antarctic contribution in 2100 is 1.14 ± 0.36 metre, and this further rises to 15.65 ± 2.00 metre by 2500 (Deconto and Pollard, 2016). In comparison, the future contribution from glaciers is small, since the total water volume stored on land based glaciers is just 0.34 metre. Besides this, the contribution from the expansion of the warming sea water is straightforward to calculate and is also projected to be limited to 0.19 metre by 2100 (under RCP 4.5). The Greenland ice sheet stores an additional 7 metre of GMSL rise, but its future contribution is also less uncertain and is not expected to exceed 0.20 metre by 2100 (Oppenheimer et al., 2019). It is the uncertainty of the tipping point at Antarctica that creates such a large spread in GMSL rise predictions. Another aspect of the possible large scale melt on the Antarctic ice sheet is the irreversibility. Once the breakup of the ice shelves has taken place, relatively warm ocean water could prevent the regrowth of the ice shelves during the coming centuries (Deconto and Pollard, 2016).

The contribution of Antarctica to GMSL rise can be roughly divided into four processes of which three are interlinked: (a) direct meltwater discharge into the ocean, (b) accelerated discharge of glaciers into the ocean and (c) ice shelf collapse (Bell et al., 2018). A fourth process is basal melting, when relative warm ocean water

causes the bottom of ice shelves to melt and the grounding line to retreat (Pritchard et al., 2012).

The first three interlinked processes are all dependent on the possible pathways of present meltwater.

a) Ice shelf collapse can be caused by meltwater lakes creating and deepening fractures in the ice shelf. Due to the additional loading of the ponded water, the ice shelf flexes downwards. After a drainage event of the lake, the loading is removed and the ice shelf flexes upwards again. This creates additional stresses in the ice shelf and causes cracks to form. Pre-existing fractures could be a location where water accumulates. When a fracture fills up, the hydrostatic pressure developed can widen and deepen the fracture, possibly all the way through the ice shelf, causing it to collapse (Bell et al., 2018).

b) When meltwater is injected into the ice sheet, it can end up at the interface between bed rock and ice sheet. Here, the meltwater could act as a lubricant, diminishing the friction between the ice and bed rock and thus accelerating the ice flow downstream (Bell et al., 2018).

c) Surface meltwater forming a network of streams and lakes could potentially drain into the ocean, either through a river terminating at the edge of the ice shelf, or through draining into a moulin^{*}, slowing the weakening of ice shelves. On the other hand the water surfaces have a lower albedo than the surrounding ice and thus create a feedback loop where surface ablation^{*} is enhanced by a higher long wave radiation uptake, resulting in more melt (Bell et al., 2018).

1.4.1. Seasonal development of meltwater networks

Although the occurrence of extensive meltwater has long been thought to be mainly focused on the Antarctic Peninsula, multiple studies (e.g. Langley et al. (2016), Kingslake et al. (2017a) and Stokes et al. (2019)) show that surface meltwater features are widespread outside the peninsula as well. Lakes present on ice shelves may cause them to break up. It is argued that the disintegration of the Larsen B ice shelf in 2002 was caused by the rapid drainage of the numerous surface lakes and the consequent hydrofractures throughout the entire shelf (Banwell et al., 2013). With a further spread of meltwater features across Antarctica, the stability of the ice shelves is therefore questioned. However, when separate lakes evolve into a connected drainage system which transports water to the ocean, the occurrence of meltwater features could actually become a stabilizing mechanism (Bell et al., 2017). Instead of forming meltwater ponds on the ice shelf, the major part of the volume of water, and thus weight of the water, could be removed from the ice shelf through such a drainage system (Bell et al., 2017). Kingslake et al. (2017a) showed that connected systems transporting water up to 120 kilometres are present all around Antarctica, but not every system will drain into the ocean. To further improve projections of GMSL rise, it would be beneficial to have an indication about which ice shelves have the potential to facilitate meltwater networks draining into the ocean and which do not. So far, the first steps are being taken around the world. Buzzard (Buzzard et al. (2018) and Buzzard and Robel (2019)) focussed on modelling the formation of lakes based on a mathematical model, including 3D processes such as water routing and channel erosion. Another approach taken is processing satellite imagery to analyse present meltwater networks, such as done by Dell et al. (2020). In her work, the meltwater network present on the Nivlisen ice shelf is digitized to study its development during the austral summer^{*}. This work could be further expanded by including topographical information of the ice shelf and comparing the results to a regional climate model.

1.4.2. Topography and routing

A digital elevation model (DEM^{*}) captures the topography of an area in a grid of cells. In hydrology, such a DEM can be used to automatically extract a potential flow routing network (an expected course for a river based on the topography of the area) using a flow routing algorithm. These routing algorithms are all based on the principle that water flows from one cell to the lowest neighbouring cell (O'Callaghan and Mark, 1984). The simple algorithms were soon expanded by no longer restricting the flow to one cell (Single Directional Flow). Water was now allowed to be distributed towards all neighbouring cells (Multi Directional Flow) based on the ratio of slope steepness (Holmgren, 1994). This greatly increased the accuracy of routing algorithms. One problem for flow routing algorithms is coping with pits. Pits are a group of neighbouring cells that are only surrounded by cells with a higher elevation. Based on the ratio of slope steepness, water can not be transported out of this pit. A pit is either present because it reflects a true depression in the landscape or because it is erroneously introduced during the creation of the DEM. Only when a pit is in reality an end point of the water flow, for instance a lake draining underground or an endorheic lake^{*}, should the pit be kept as a depression in the routing algorithm. In all other cases, water should be allowed to leave the pit. Based on dif-

ferent thresholds, such as depth or area of a pit, a user can decide to dismiss the pit or keep it as an endpoint for the flow routing algorithm. Research shows that the resulting potential routing network is very sensitive to the thresholds used: the density and connectivity of a routing network are easily over- or underestimated when using a different threshold value (Yang et al., 2015). Once a pit is flagged as an error, flow routing algorithms generally fill the pit. By raising the elevation of the pit, the DEM itself is altered until water is able to escape the pit somewhere. This results in large flat areas in the DEM over which the flow is routed, often in a straight line. This possibly introduces errors in the resulting potential flow routing network (Metz et al., 2011). An alternative algorithm does not fill the found pits, but uses a least cost path algorithm. Using the elevation of a cell as its cost, flow is routed over the least expensive cells (Ehlschlaeger, 1989). In this way, the original elevation data is not affected. The algorithm has proven to be both faster and more accurate than pit filling algorithms (Metz et al., 2011).

A potential flow routing network on a certain location alone does not guarantee the occurrence of rivers and lakes, a water source is needed as well. A combination of water supplied and the potential routing network gives a good indication of the location of a water network. Precipitation and groundwater are the sources for river systems for traditional land based hydrology. However, on Antarctica water is mainly provided through the melt of snow and ice. Thus to further study the occurrence of meltwater features on an Antarctic ice shelf, snowmelt and refreezing data should be included. This data can be found in regional climate models.

1.4.3. Climate data

Only little field measurements are available on Antarctica because of the harsh environment and remote location. Therefore, modelling of Antarctic processes often relies on data from climate models. Global climate models have a relative coarse resolution and are thus not suited for further modelling of smaller scale processes. Regional climate models solve this issue. These models, with a resolution up to a couple of kilometres, are able to capture local topography and provide climate data on a finer scale. They are coupled to the global climate models at their boundaries, but resolve the area of interest independently. For Antarctica, the regional atmospheric climate model (RACMO) produces various climate variables on a 5.5 x 5.5 kilometre resolution (van Wessem et al., 2018). Two of the climate variables one should take into account while studying melt water feature development are snowmelt and refreezing rate. The snowmelt rate is driven by the energy balance on the interface between the atmosphere and the firn layer* (the top layer on ice shelves, which is a mixture of ice and snow). The energy balance includes short wave radiation, long wave radiation, sensible heat, latent heat and energy supplied by rainfall (Bougamont et al., 2005). The albedo of the surface determines how much of the incoming short wave radiation is reflected. A bright surface (ice or snow) has a higher albedo than a darker surface (water) and thus ice reflects more of the incoming short wave radiation than water does (Bougamont et al., 2005). The long wave radiation is partly absorbed, but also emitted following the Stefan-Boltzman constant (Bougamont et al., 2005). The balance is further complemented by including sensible heat, latent heat and a small source of energy supplied by rainfall (Bougamont et al. (2005) and Ettema et al. (2010)). Liquid water infiltrates down into the firn layer as long as the density of the firn layer does not exceed 910 kg/m³. If the density is larger, water is not able to infiltrate and will start to pond on the surface, or flow over or through the firn. The density of firn is variable over time, because of the settling of the firn layer and the refreezing of water within (Ettema et al., 2010). The amount of water that refreezes is determined by three factors: the water available, the pore space and the temperature. Water only refreezes as long as the ambient temperature is staying below the melting point. The ambient temperature also changes during the freezing process due to the release of heat during the transition of water from the liquid to the solid phase (Ligtenberg et al. (2011) and Ettema et al. (2010)). As long as the firn layer is thick enough and enough pore space is available for melted water to infiltrate and percolate, the refreezing will continue. Over time, refreezing does lower the firn air content, but new snowfall on top of the firn layer will also add new pore space at the same time. Only when the net change in firn air content is below zero and the firn air content drops to zero, water will no longer be able to percolate down and start to accumulate on the surface (Kuipers Munneke et al., 2014). Unless an ice layer forms close to the surface due to the refreezing of meltwater. This also prevents water from percolating further down (Buzzard et al., 2018).

The spatial pattern of the surface melt product of RACMO correlates well with observations, but the absolute values can be 30-50% lower than those observed (Lenaerts et al., 2017). Especially close to grounding lines, the surface melt can be underestimated in RACMO due to an enhanced albedo-melt feedback influenced by persistent katabatic winds*. Air flows from the higher regions down towards the ice shelf and warms

during the decent. This can cause the temperature to rise 3°C. Additionally, these winds erode the snow layer, exposing blue ice areas (Lenaerts et al., 2018). Research shows that the underestimation of snowmelt is likely caused by a misrepresentation of the albedo-melt feedback (van Wessem et al., 2018). The quick change in albedo values when a surface becomes wet or when new snow covers bare ice is difficult to capture and possibly explains this misrepresentation (Ettema et al., 2010).

Combining climate, topographical and satellite data, this research will present an analysis of the meltwater network present on the Nivlisen ice shelf during the melting season of 2016-2017.

This thesis consists of four chapters. Chapter 1 gave an introduction into the thesis topic, presented the three questions of this research and described the theoretical framework. Chapters 2 (method) and 3 (results and discussion) will in general be divided into three parts corresponding to the three questions and their topic: 1) satellite observations of the development of meltwater features, 2) the influence of the topography on the shape and extent of meltwater features and 3) the use of climate data to explain the found location of meltwater features.

Chapter 2 (Method) starts with a description of the study area (section 2.1). Thereafter the sections containing the method for satellite observations (section 2.2), topography and routing algorithms (section 2.3) and climate data (section 2.4) can be found.

Chapter 3 (Results and Discussion) starts with the same three topics: Meltwater observations (section 3.1), Topography (section 3.2) and Climate data (section 3.3). The discussion for each of these topics can be found directly after the results are presented for each topic. Afterwards one can find a section where the results are described from the additional analysis that was executed for the Roi Baudouin ice shelf and the corresponding discussion (section 3.4). Chapter 3 concludes with a general discussion where all results are combined (section 3.5).

Chapter 4 (Conclusions and Recommendations) first shortly summarizes the obtained results and answers the three questions. This chapter and this thesis ends with recommendations for further studies and possible improvements.

2

Method

This chapter starts with describing the chosen study area and continues with explaining the chosen or developed methods to find an answer to each of the three questions posed in section 1.3.

2.1. Study area

The Nivlisen ice shelf is located in Dronning Maud Land on the East Antarctic ice sheet (Figure 2.1.a). The ice shelf spans roughly 80 kilometres from its grounding line towards the ocean and has a width of 130 kilometres. The ice shelf gently slopes upwards ($5 * 10^{-4}$) from 40 metres near the ocean to 80 metres close to the grounding line, where the floating ice shelf becomes grounded on solid rock. From the grounding line the land rises more steeply towards a plateau of 100 metres and higher (Figure 2.1.b). The ice shelf is typically 150 to 700 metres thick and the ice flows with a speed in the order of 100 metres per year (Horwath et al., 2006). This ice shelf was chosen as the study area, since climate data (see section 2.4 for further elaboration) was available for this location. Furthermore, observations of meltwater features on this ice shelf were documented in multiple studies (Kingslake et al. (2017a) and Stokes et al. (2019)).

Halfway through this study, it was decided that including a second ice shelf for an additional but partial analysis would be beneficial. The Roi Baudouin ice shelf is also located within Dronning Maud Land and the same climate data, satellite observations and DEM as for the Nivlisen ice shelf were available on the Roi Baudouin ice shelf. Meltwater features had previously been observed, both in satellite observations (e.g. Kingslake et al. (2017a) and Stokes et al. (2019)) and during field expeditions (Lenaerts et al., 2017).

It was chosen to study the summer of 2016-2017, because this was the only summer covered by both Sentinel 2, Landsat 8 and RACMO data.

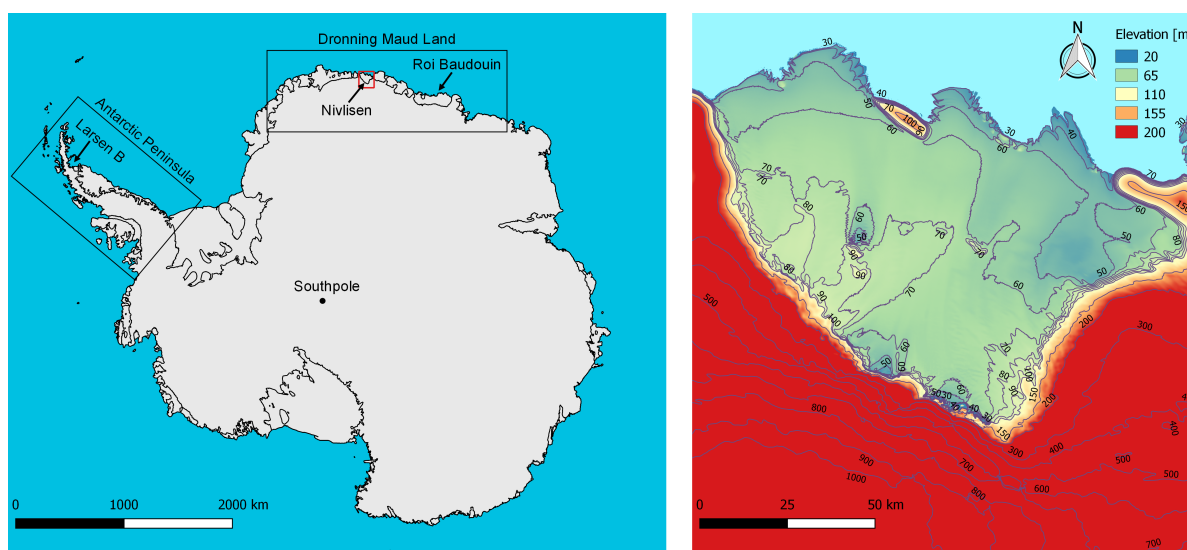


Figure 2.1: (a) Overview of Antarctica and (b) the elevation of the Nivlisen ice shelf.

2.2. Observations

2.2.1. Satellite data

Two optical satellites were used for this study, Sentinel 2 and Landsat 8. They have a resolution of 20 and 30 metres, respectively. Twelve cloud free scenes were selected from December 1st 2016 to March 31st 2017 (Table 2.1). The true colour image (combining the red, green and blue bands per scene) are used for the digitization step.

Table 2.1: Dates used in this study. This is based on the cloud free satellite imagery obtained from Landsat 8 and Sentinel 2.

Dates of timesteps used in this study			
2016-12-04	2016-12-27	2017-01-19	2017-02-13
2016-12-11	2017-01-05	2017-01-26	2017-02-25
2016-12-17	2017-01-12	2017-02-04	2017-03-24

2.2.2. Digitization

For each time step observed, meltwater features were manually digitized using the Google Earth Engine Digitisation Tool (Lea, 2018) where one can draw polygons in satellite imagery by hand and download these polygons for further analyses. Consequently, the meltwater features were imported to QGIS and the area was calculated using the native QGIS functionalities.

2.2.3. Depth and volume calculations

To obtain an estimate for the depth of the meltwater features, a DEM was used. The Reference Elevation Model of Antarctica (REMA) provides the elevation of the Antarctic ice sheet on an eight metre resolution. It was created by the Polar Geospatial Center of the University of Minnesota (Howat et al., 2018). The elevation model was combined with the meltwater feature area to obtain the mean depth and the volume of the meltwater network (Figure 2.2 and Figure 2.3). The elevation from REMA was sampled along the border and the centreline of all meltwater features on a 50 metre interval. The centreline was created using the QGIS plugin 'Geometric Attributes' created by Nyberg et al. (2015). A buffer of 50 metres was applied to the points on the centreline, to account for deeper parts adjacent to the exact location of the centreline. The maximum depth was then calculated by taking the difference between the elevation of a point on the border and the elevation of the closest point on the centreline. By dividing the average of all maximum depths by two, the mean depth was calculated. This assumes a triangular shape of the cross section. Finally the mean depth was multiplied with the area, obtaining the calculated volume of the observed melt water features.

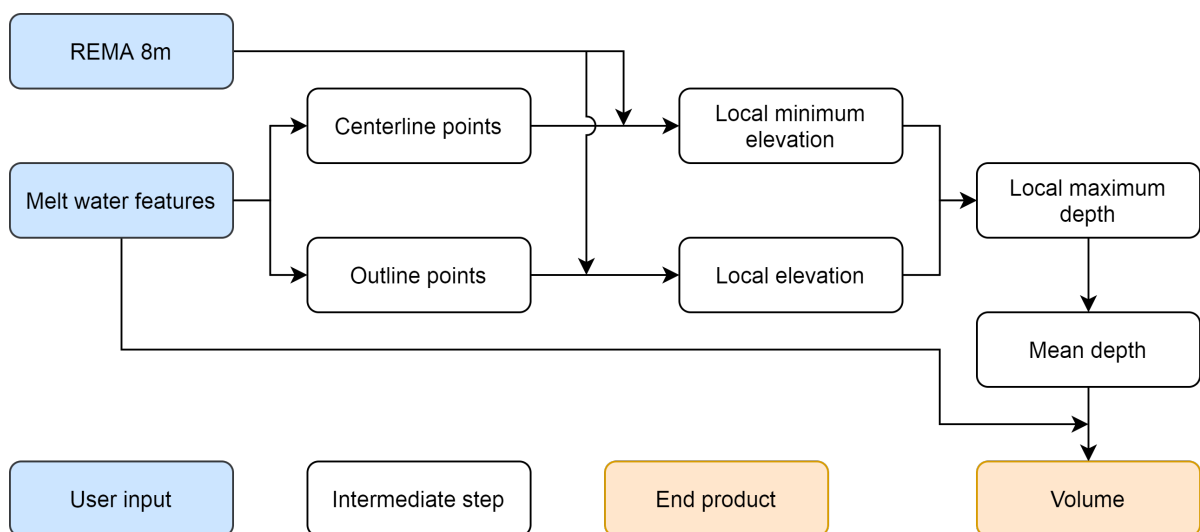


Figure 2.2: Flow diagram for depth and volume calculations.

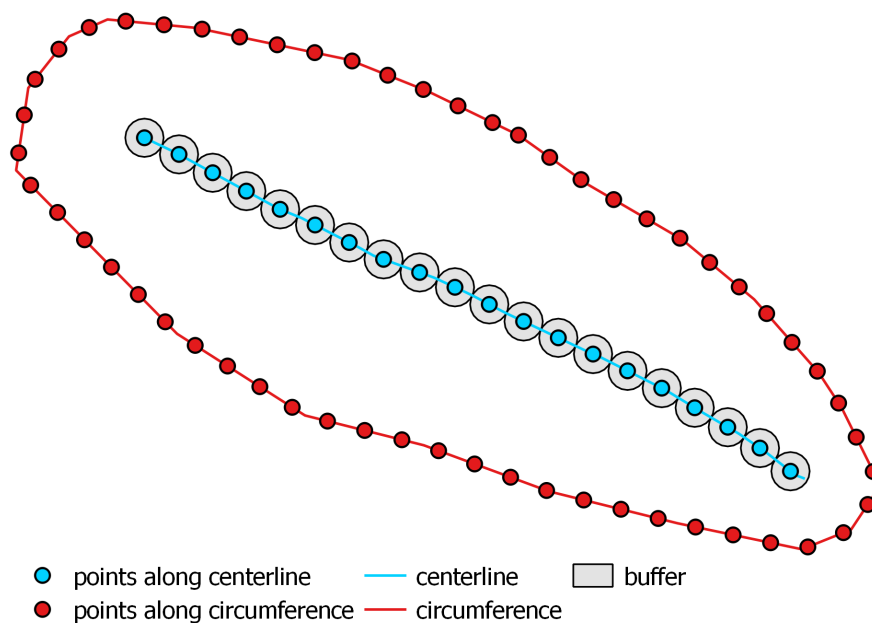


Figure 2.3: The used features for one meltwater lake to calculate the mean depth. Points along the circumference sample the elevation on that point. Points on the centreline sample the minimum elevation within an area around the point. The depth is calculated for every point on the centreline as the difference with the elevation from the closest point on the circumference.

2.2.4. Comparison to Dell (2020)

As a validation step, the calculated areas, depths and volumes were compared to the research done by Dell et al. (2020). In her research the Normalised Difference Water Index (NDWI) was used to automatically identify water bodies. The NDWI is the normalised ratio between the blue and red band from the satellite imagery, which has a large contrast between ice and water. The resulting water mask was filtered to only keep water bodies larger than 1800 m². Depth calculations are based on the light attenuation in the water column by comparing the reflectance of a pixel in a lake to the reflectance of optically deep water pixels in the ocean (Dell et al., 2020).

2.3. Routing

Using an ‘of the shelf’ algorithm to obtain a potential routing network for an Antarctic ice shelf did not give sufficient results. Traditional pit filling algorithms would yield sufficient results when used on exorheic* catchments, since the outflow point is always the open sea or ocean. But once applied on an endorheic basin, flow is still forced towards the ocean. The observed meltwater features on the Nivlisen ice shelf are all part of an endorheic basin, there is no outflow point at the ice shelf cliff. Instead, river systems end in a lake at the deepest part of larger depressions (Figure 3.1). If nevertheless all depressions were to be filled, a fully connected system would be created, terminating in the ocean, which is not what was observed in reality. Accounting for this by allowing all pits do be an endpoint for a routing algorithm would result in a routing network consisting of short and isolated channels terminating in (small) depressions. An intermediate solution was required to accommodate networks terminating in real depressions and thus forming networks that are not overly connected, but also not too separate. Moreover, when depressions with very large areas occur, not the entire depression can be marked as such. Otherwise, routing networks would stop as soon as they enter a depression, causing the loss of routing information once inside. Only the deepest part of depressions should be kept as an endpoint. Besides this, the algorithm has to be able to cope with the low slopes present at Antarctic ice shelves. These criteria are all met in the workflow proposed in this study (Figure 2.4) using freely available programs and algorithms. The core of the method is the A^T algorithm, part of the r.watershed function within QGIS-GRASS 7.0. This algorithm is shown to perform better on relatively flat surfaces compared to other routing algorithms (Kinner et al., 2005). The A^T algorithm does not fill depressions to route flow, preserving the original DEM and thus giving more details to the resulting routing network (Ehlschlaeger, 1989).

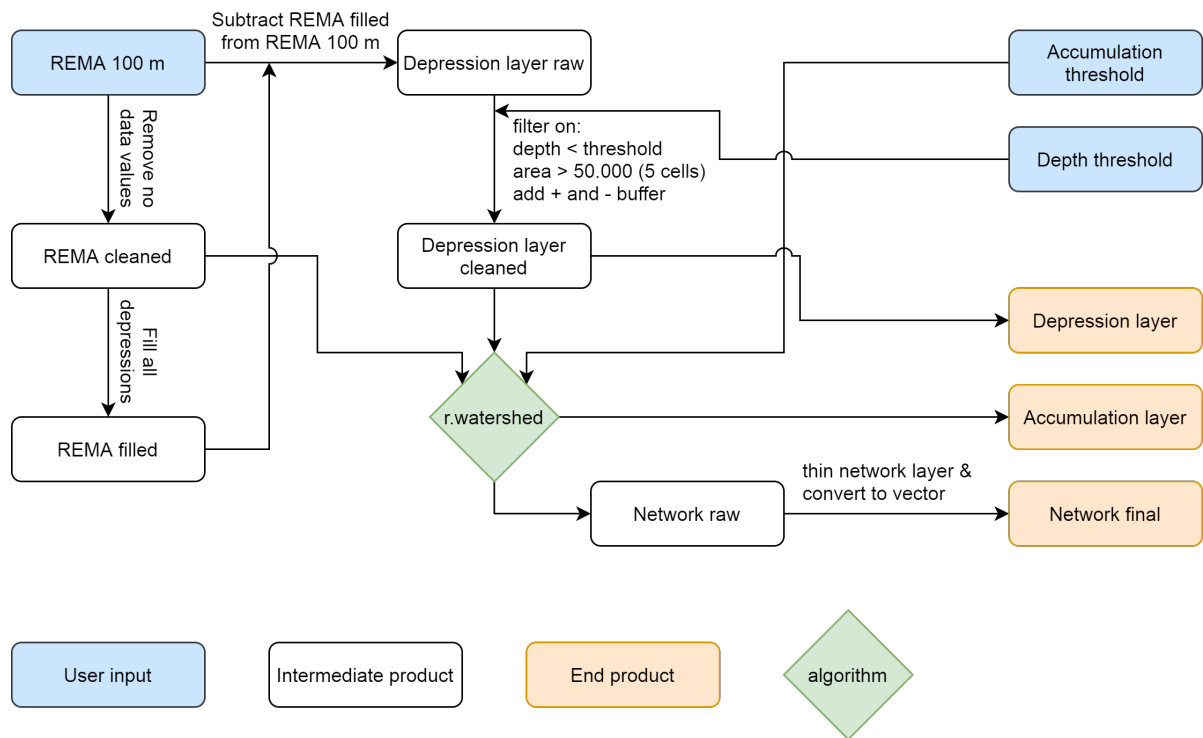


Figure 2.4: Flow diagram for the routing method proposed in this study.

The algorithm needs an accumulation threshold, a DEM and the layer containing the depressions mentioned above. The 100 metre resolution product of REMA was used as input for the created routing method. This proved to yield similar results as the 8 metre resolution product and resulted in shorter calculation times. To create a raw depression layer (a first layer that still needs some filter steps to complete), the no data values (equal to $-3.4028230607370965e38$) from REMA were removed first. Without removing these values, the routing algorithm would try to also create routing networks over the ocean or data gaps. The resulting cleaned REMA layer was consequently filled using the `r.fill` algorithm (part of QGIS-GRASS 7.0). This filling algorithm needs several loops to completely fill REMA until every depression is resolved (GRASS Development team, 2020). During this study it was found that six loops were sufficient to completely fill both of the two ice shelves considered. A completely filled DEM no longer has pits without outflow points, each cell is able to drain somewhere. By subtracting the filled REMA layer from the original REMA layer, the raw depression layer was created. As described before, using every depression found in REMA for the routing algorithm, would not yield accurate results. Therefore, two filter steps were needed to obtain a depression layer that could be used in the routing algorithm. Depressions more shallow than the chosen depth threshold were discarded, keeping only the deepest depressions. For the Nivlisen ice shelf, a depth threshold of 9.5 metre yielded the best results. This value should be selected by trial and error for every new location where this method would be applied. Furthermore, only depressions consisting of more than five cells (or 50.000 m^2) are preserved for the cleaned depression layer. Finally, a positive and then a negative buffer of 100 metre were applied on all depression features to resolve possible inconsistencies in the shape file. The resulting cleaned depression layer was one of the three inputs for the `r.watershed` algorithm. A complete graphical overview of the method implemented in QGIS can be found in Appendix A.3, Figure A.2. The second input for the `r.watershed` algorithm was the cleaned REMA layer and thirdly an accumulation threshold was defined. This last threshold determines how many cells have to drain through one particular cell to mark it as part of a routing network. Lowering this threshold will create a more dense network, whereas a higher threshold will only keep main branches. An accumulation threshold of 10.000 gave the right balance between a too sparse and too dense routing network.

The `r.watershed` algorithm, using the Multiple Directional Flow A^T algorithm explained above, takes the DEM, depression layer and the accumulation threshold as input and generates multiple output layers. Two of these layers were further used. The accumulation layer contains the number of cells draining to the cell under con-

sideration. The stream segment layer, or the raw network layer in Figure 2.4, includes all stream segments identified. This raster layer was firstly thinned to create linear features of one cell width. Finally it was converted to a vector layer for better visualization. This final network layer containing all streams was further studied and the results were presented in section 3.2.

2.4. Climate data

To study the underlying physical drivers, data from RACMO was used. This model provides data on a daily basis with a resolution of 5.5 kilometres. In this study, snowmelt, refreezing, temperature and incoming short wave radiation datasets were used (van Wessem et al., 2018). Important to take into account is the reliability of the data. Two studies (Lenaerts et al. (2017) and Lenaerts et al. (2018)) showed that RACMO data can underestimate surface melt by 30 to 50 % and especially close to grounding lines the deviation from observations can be large.

As a first step in studying the climate data, the Pearson correlation coefficients for two drivers of snowmelt, temperature and incoming short wave radiation, and the calculated volume of the meltwater features were calculated. The Pearson correlation coefficient is a value between -1 and +1. Two positive linear correlating datasets will have a coefficient of +1, whereas no correlation would give a coefficient of 0. A coefficient of -1 indicates a negative linear correlation. This might give an indication of the existence of a clear link between the temperature and incoming short wave radiation as modelled by RACMO and the observations of meltwater features on the Nivlisen ice shelf.

Afterwards, the melting and refreezing product of RACMO were analysed to study spatial and temporal patterns in the modelled snowmelt and compare this to the observations of meltwater features. The temporal mean snowmelt and refreezing rates were calculated for every time step between the dates corresponding to the cloud free scenes selected from the satellite data. All time steps were then exported to QGIS where only the melt and refreezing data within the catchment area of the observed meltwater features was kept. Data outside this catchment area was discarded for the water balance. A simple water balance was made per pixel: $Q = P - RF$, where Q is the nett modelled meltwater production, P is snowmelt and RF is refreezing. All units were initially millimetres per timestep, but were converted to cubic metres per timestep to match the calculated volumes of observed meltwater features. Lastly, Q was summed over all pixels within the catchment to obtain the total amount of nett modelled meltwater produced, which was then compared to the change in volume of the observed meltwater network during each time step. As explained in section 3.3.2, the integrated snowmelt and refreeze rates did not match the meltwater volume calculated based on observations. Therefore, also the daily snowmelt and refreeze rates were studied. Days when snowmelt exceeded the refreeze rate were marked and summed. The spatial pattern of these days was then compared to the observations of meltwater features.

3

Results and Discussion

This chapter presents and discusses the obtained results. For each topic separately, the results are presented and directly discussed. The first section (section 3.1) contains the results from the satellite observations of meltwater features. The area, depth and volume of the meltwater features are calculated based on the satellite imagery and a digital elevation model. Section 3.2 then presents the results from the routing algorithm, where a digital elevation model is used to create potential routing networks on the Nivlisen ice shelf. Thirdly, section 3.3 shows the results from studying the climate data from the Regional Atmospheric Climate Model. Afterwards, a partial analysis was executed for the Roi Baudouin ice shelf and the results can be found in section 3.4. Finally, this chapter finishes with a general discussion, where all results are integrated and discussed together in section 3.5.

3.1. Meltwater observation

Using satellite data from two optical satellites, the extent of meltwater features on the Nivlisen ice shelf were digitized. The area was calculated for all meltwater features. By combining this with the Reference Elevation Model of Antarctica, the depth and consequently volume were calculated. This data was compared to a study in which the volume, depth and area of the meltwater features present on the Nivlisen ice shelf in the melting season of 2016-2017 were calculated as well (Dell et al., 2020). The results are presented below and discussed in section 3.1.4.

3.1.1. Area

The maximum area of the meltwater network on the Nivlisen ice shelf occurred on 2017-01-19, when $1.64 \cdot 10^8$ m² of water was observed (Figure 3.1). Three areas were identified: individual lakes at higher elevations, a dense and connected network in the southern part of the ice shelf and a more linear part stretching north. The network encompassed approximately 40 kilometres in both South-North and East-West direction. An overview of the meltwater extent for all dates can be found in Appendix A.3, Figure A.1. The meltwater channels did not widen significantly over time, but lakes did increase in size and were connected by forming additional meltwater channels throughout the melting season. The area stayed below $2.55 \cdot 10^7$ m² until 2016-12-11 and increased during the end of December and the beginning of January to the maximum value of $1.64 \cdot 10^8$ m² on 2017-01-19. It gradually declined to zero by April (Figure 3.2.a). By combining all dates in one figure, the movement of the front of the meltwater network was visualized (Figure 3.3). The meltwater front of the western system moved with a speed of about 5 kilometres per week (or 0.5 metre per minute). The first melt water features occurred on 2016-12-04 close to the grounding line in the south part of the ice shelf. One week later (2016-12-11), melt water features developed throughout the south part of the ice shelf, but only as separate lakes. By 2016-12-17, the first features were connected and started forming melt water networks, which started to expand northward from 2016-12-27 onward. After the maximum was reached on 2017-01-19, the melt water features shrank in size or were frozen over until only a couple features remained on 2017-03-24 (Figure A.1, Appendix A.3).

3.1.2. Depth and volume

The calculated mean depth of the meltwater network did not change significantly over time, but varied between 0.23 and 0.27 metre. 90% of the calculated depths were between 0.05 and 0.67 metre, except for 2017-03-24 when the calculated mean depth was 0.48 metre (Figure 3.2.b). The deepest melt water features are found close to the grounding line in between exposed bed rock formations. Combining the calculated

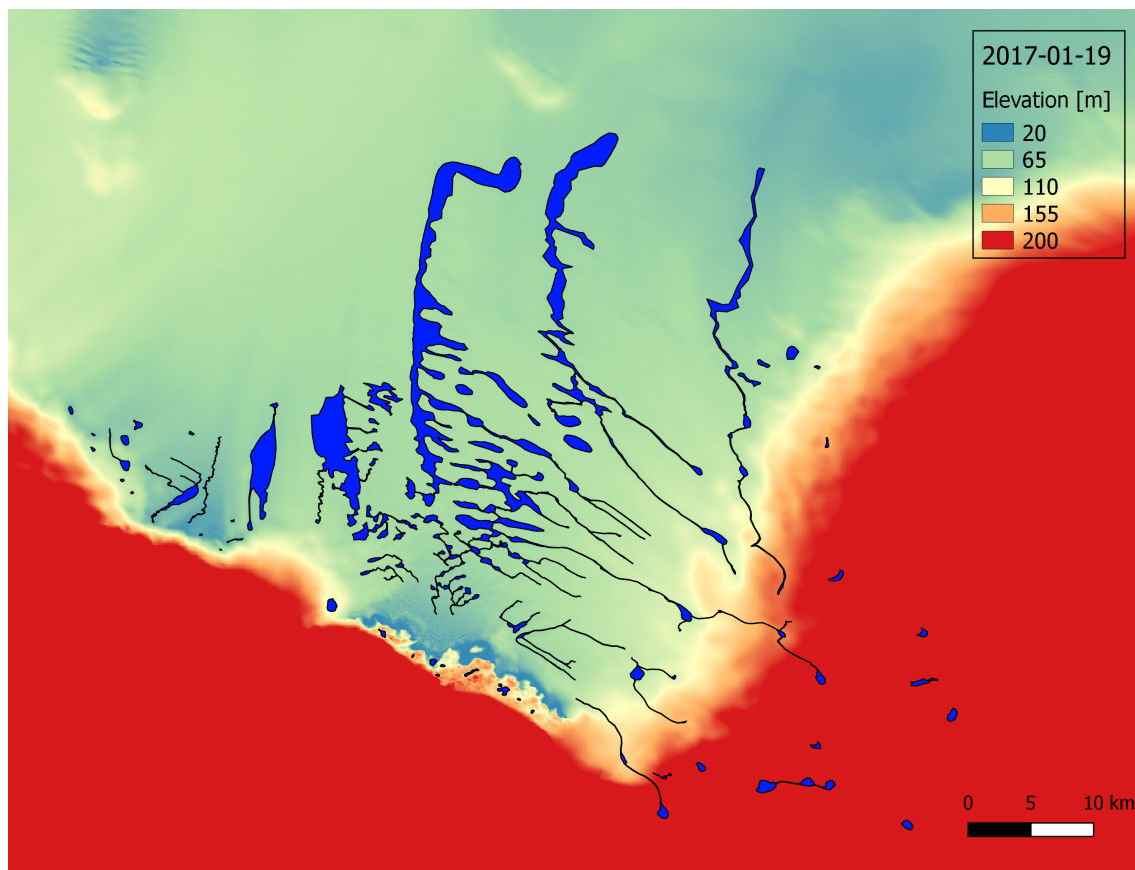


Figure 3.1: The maximum water extent reached in the 2016-2017 melt season on 2017-01-19.

mean depth and area resulted in the volume of the meltwater network. The calculated meltwater volume had a steep rise between 2016-12-11 and 2016-12-17 and gradually shrunk after the maximum was reached on 2017-01-12, with a total of $3.8 \cdot 10^7 \text{ m}^3$ (Figure 3.2.c).

3.1.3. Comparison to Dell et al. (2020)

Dell et al. (2020) also determined the volume of the same meltwater network for the 2016-2017 melt season. Her results were compared with the calculated meltwater volume. The relative difference between the volumes ranges from -85% to +125% (Figure 3.2.c). These two large deviations occurred during the last two time steps (2017-02-25 and 2017-03-24). The timing of the maxima, minima and the increase and decrease of the calculated meltwater volume did coincide, although the absolute values differ. The depths found by Dell et al. (2020) are larger than those found in this study. However, the method to determine the area of the meltwater networks used by Dell et al. (2020) resulted in smaller areas found. This is further discussed in section 3.1.4.

3.1.4. Discussion

By manually delineating meltwater features during the digitization step, an error was introduced by the subjectivity of the user. It is possible that either too many or too few areas are classified as meltwater feature because of this user bias. Research suggests that the user bias was found to be very small during a digitization process (Keefer, 1988), although this did not specify whether the digitized features were hard to distinguish from the surrounding area. Therefore, the potential error introduced during digitization was not significant for the results of this study. An approach for delineating meltwater features automatically was created by Yang and Smith (2013). A normalized difference water index, specifically for icy areas ($NDWI_{ice}$), is calculated by taking the normalized difference of the red and blue band from optical satellite imagery: $NDWI_{ice} = (Blue - Red) / (Blue + Red)$ (Yang and Smith, 2013). While this method is more practical to use when analysing a larger (either spatially or temporally) dataset, it is also limited by two factors. Firstly, the resulting meltwater features are very sensitive to the threshold distinguishing between water, ice and slush

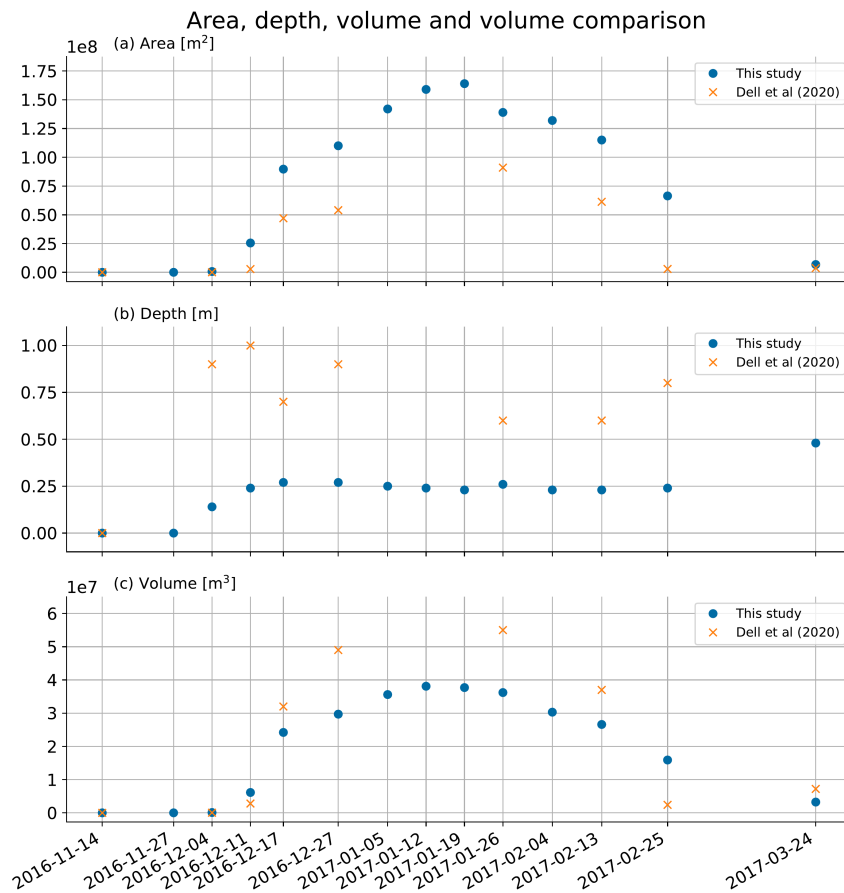


Figure 3.2: (a) The change of observed meltwater area from December 2016 to March 2017. This study found larger areas in comparison to Dell et al. (2020), but the timing of the found maxima and the first observations of meltwater features were similar. (b) The change of calculated meltwater depth from December 2016 to March 2017. Dell et al. (2020) found larger depths using a depth calculation based on the light attenuation in the water column, whereas depth calculations in this study were based on a DEM. (c) The change of calculated meltwater volume from December 2016 to March 2017. The calculated depths in this study are somewhat smaller than the depths calculated by Dell et al. (2020). But timing of the maxima and the general development of the calculated volumes is quite similar. The area, depth and volume derived by Dell et al. (2020) is included in orange crosses in each figure.

(a water and ice mixture). A small change in chosen parameters leads to large differences in the end product (Banwell et al., 2014). Secondly, meltwater features that are partly frozen over introduce an underestimation of the total meltwater area (Banwell et al., 2014). Dell et al. (2020) used such an automated process to delineate meltwater features. The possibility of errors in this method was reflected in the increase of meltwater volume in the last time step while no meltwater was produced during the corresponding period. Large differences between the calculated volumes in this study and by Dell et al. (2020) were found during the last two timesteps of the meltwater observations. Dell et al. (2020) derived a very small area on 2017-02-25 and calculated a large depth (2 metres) on 2017-03-24. On 2017-02-25, satellite imagery showed a first onset of refreezing of the top of the meltwater features and some light cloud cover was present. The meltwater features were still classified as meltwater by hand in this study and the clouds were thin enough to trace the meltwater features in the clouded area. It is possible that the method using the $NDWI_{ice}$ as described above, did not capture both the meltwater features that had started to refreeze and the meltwater features under the thin cloud cover. Considering this, the derived volumes of the observed meltwater features in this study were thought to be in line with the findings by Dell et al. (2020).

The method to determine the depth of meltwater features in this study was based on a static DEM. There-

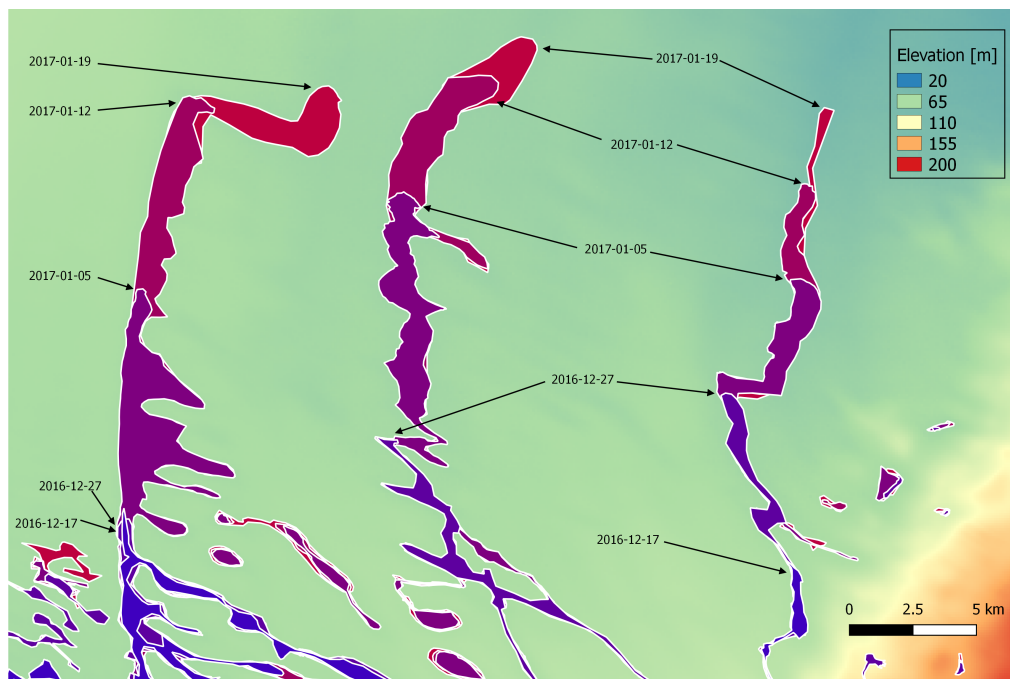


Figure 3.3: The progression of the meltwater front during the 2016-2017 melt season. The colours blue to red each represent timesteps corresponding to the dates listed in the figure. The front moved roughly 5 kilometres during each time step of 7 days.

fore, the continuous flow of the ice shelf was not included, possibly causing an offset of the location of the deepest parts of a meltwater feature. Moreover, dynamical processes, such as thermal erosion of the channels caused by the higher temperature of the meltwater transported (Marston, 1983), were not taken into account. Hence calculated meltwater feature depths might be underestimations of the true depth. Lake bottoms become deeper by the positive albedo feedback of the darker surface of the meltwater lake in comparison to the ice/snow cover around it, thus absorbing more radiation. This can account for up to 135% increase in ablation rate of the lake in comparison to its surroundings (Tedesco et al., 2012). The effect of the movement of the ice shelf and thermal erosion will become larger as the DEM used becomes older. Using the light attenuation in the water column to calculate water depth (e.g Sneed and Hamilton (2007) & Dell et al. (2020)) would mitigate these problems but was not validated on the Antarctic ice sheet. As with area calculations, the depth of meltwater features partly covered with ice can not be retrieved (Banwell et al., 2014). Moussavi et al. (2020) have developed a method to generate meltwater volumes and area over large temporal and spatial scales, while improving the overall accuracies. This could greatly enhance the possibilities of studying meltwater features during multiple seasons and over larger scales.

Another point to reflect on is the slow movement of the front of the meltwater network. The size (67.0 km^2) and progression (0.5 metre per minute) of the observed melt water feature on the Nivlisen ice shelf resembles the behaviour of the largest meltwater feature on the Amery ice shelf during the summer of 2014-2015 as found by Kingslake et al. (2017a). This front moved with a speed ranging from 0.8 to 2.5 metre per minute and had a total area of 56.7 km^2 (Kingslake et al., 2017a). Velocities in the order of a metre per minute are very low for unrestricted surface streams. Flow velocities measured on the Greenland ice sheet were 0.4-2.6 m/s (Gleason et al., 2016). As a further comparison, the Manning equation was used to derive a typical flow speed for freely flowing water, formula 3.1 (Manning, 1891).

$$V = \frac{R^{2/3} \cdot \sqrt{S}}{n} \quad (3.1)$$

V is the calculated flow velocity in m/s. R is the hydraulic radius in metres, calculated as the cross sectional area divided by the wetted perimeter. R can be approximated as the stream depth for wide channels. S is the (average) gradient of the stream bed. Lastly, n [$\text{s}/\text{m}^{1/3}$] represents the Manning roughness coefficient, a measure for how smooth or rough a stream bed is (Manning, 1891). When assuming a depth of 0.25 metre (the average depth found in this study), an average gradient of $5 \cdot 10^4$ and a smooth ice stream bed, corresponding

to a Manning roughness coefficient of $0.035 \text{ s/m}^{1/3}$ (the mean value found for supraglacial* streams on the Greenland ice sheet (Gleason et al., 2016)), an expected flow velocity of 0.2 m/s was found (Manning, 1891). Movies made during a fieldwork campaign showed even larger flow velocities in the order of metres per second, albeit in smaller channels (Lenaerts and Lhermitte, 2016). Therefore it is expected that the front of the meltwater network is not a freely flowing water mass. A possible explanation for the slow movement of the front could be that water at the front was draining into the firn layer, as suggested by Stokes et al. (2019). It might be that only after the firn layer was fully saturated was it possible for meltwater to continue its path over the surface of the firn layer.

The meltwater network observed on the Nivlisen ice shelf is very different from meltwater networks on the Greenland ice sheet (GrIS). Shorter (<10 kilometre) and smaller drainage channels on the GrIS form a dense network terminating in small moulins (Yang et al., 2016), whereas the longest connected meltwater feature stretched over 70 kilometre on the Nivlisen ice shelf. A higher surface gradient of the glaciers and a higher meltwater production on the Greenland ice sheet may both be the cause of the differences observed. The meltwater features on the Nivlisen ice shelf do resemble those on other locations on Antarctica as found by Kingslake et al. (2017a): broader channels, elongated meltwater features, round or ellipsoid lakes and often with a tip where water flows out of the lake. The location of the lakes is also in line with findings by Kingslake et al. (2017a), who notes that meltwater features are often located close to exposed bed rock formations (nunatak's*) and blue ice regions (Kingslake et al., 2017a).

3.2. Topography and routing

Below one can find the results from the method developed to create a potential routing network. The Reference Elevation Model of Antarctica was used as the input for this method. Preprocessing steps were executed in order to create a potential routing network that would be as close as possible to reality. The created routing network was compared to the observed patterns of the meltwater features in section 3.2.1. Section 3.2.2 shows what happens when one does not use an optimal setting for depression thresholds. Lastly, the results are discussed in section 3.2.3.

3.2.1. Routing algorithm

The routing workflow resulted in a potential routing network for six chosen accumulation thresholds ranging from 2500 to 20.000 cells (or 25 to 200 km²). Potential routing features are present all over the ice shelf, as well as on the higher elevated grounded ice (Figure 3.4). The routing features did overlap with the main branches of the observed meltwater network in the South-Eastern part of the ice shelf. Lower threshold values introduced more side branches over the entire study area, whereas higher thresholds removed branches on the location of observed meltwater features. For the Nivlisen ice shelf, a threshold of 10.000 gave the right balance between too many side branches and a too sparse network. Additionally, a depth threshold of 9.5 metres was chosen. The four major depressions on the ice shelf had a depth of 10+ metres. Choosing a depth of 9.5 metres ensured that only the center of each depression was conserved for flow routing calculations.

3.2.2. Influence of depressions

As mentioned in section 2.3 and section 1.4.2, depth thresholds are the dominant factor for the end result of a routing algorithm (Yang et al., 2015). To illustrate this further, a potential routing network was also created for two extreme cases, in contrast to the proposed situation as presented in section 3.2. In case A, all depressions were used as potential endpoints for the routing algorithm (Figure 3.5.A). The depth threshold was manually set to -0.01 metres. The routing algorithm resulted in short channels which did not form a network. Case A did not reflect observations of meltwater features in any way. In case B, all depressions were excluded as potential endpoints. The routing algorithm was only allowed to route flow toward the ocean (Figure 3.5.B). This resulted in the formation of one very large potential network in the southern region of the ice shelf, which connected to the ocean in the North-West part of the ice shelf. Water from the southern part would thus be flowing North, to the ocean, whereas observations indicated that water flows to the depressions present in the South part of the Nivlisen ice shelf (S.L.M. Lhermitte, personal communication, October 2019). Five networks, mostly consisting of one main channel, were created by the routing algorithm left from the outflow point of the largest network. These networks were at the same location and had the same shape as the networks on those locations in the potential routing networks in Figure 3.4.

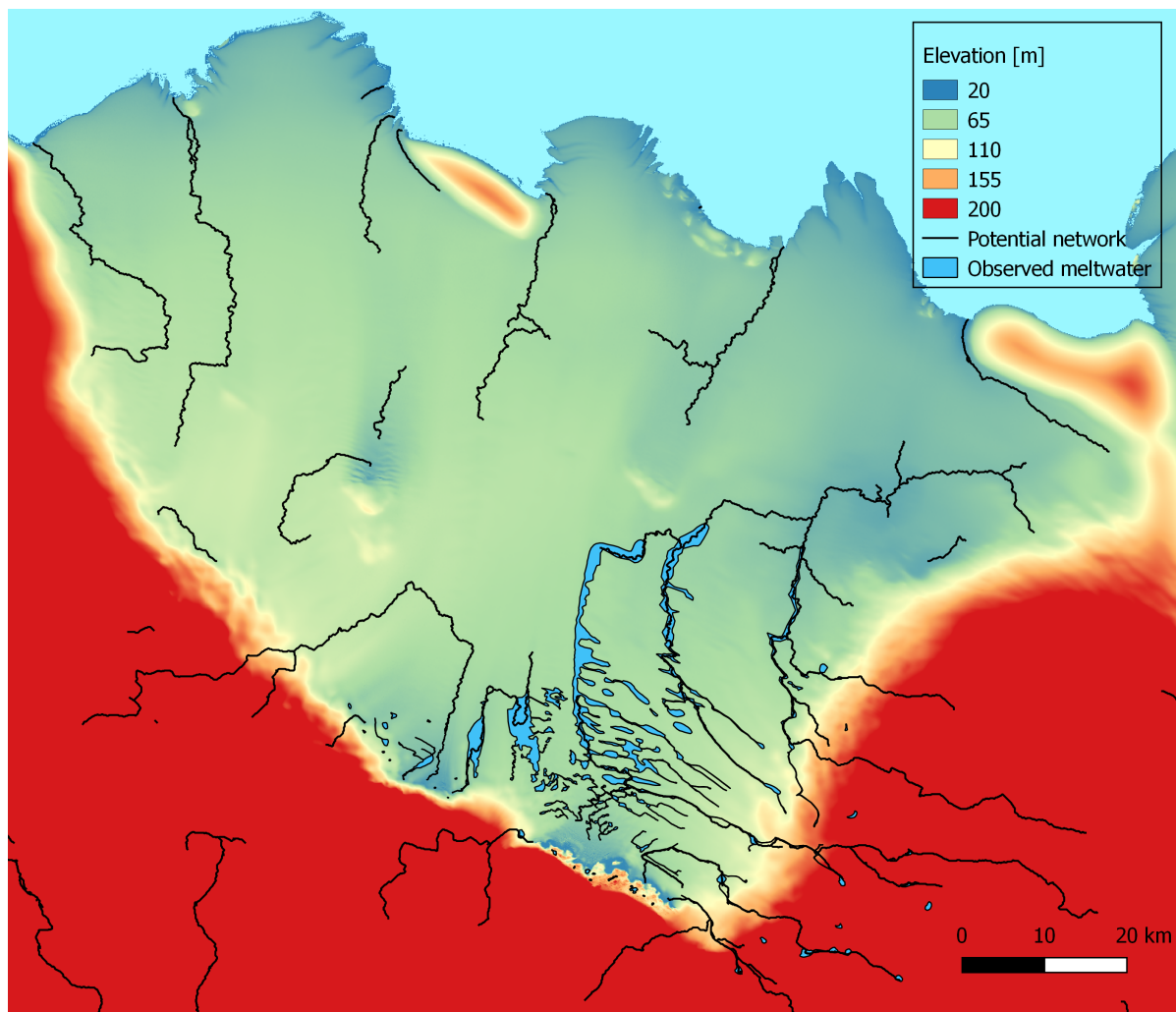


Figure 3.4: Potential routing network created with a threshold for accumulation of 10,000 cells (equal to 100 km²) and a depression threshold of -9.5 metres. Several networks are created. Some networks terminated in large depressions located in the south-east and west part of the ice shelf. Other networks located in the northern part of the ice shelf do connect to the ocean directly.

3.2.3. Discussion

While Dell et al. (2020) suggested that a "flow routing analysis is extremely hard" (response to Reviewer comments Dell et al. (2020), p.4 and p.24) when using REMA, the results of this study showed that it was possible to create a potential routing network based on REMA. The performance of the routing algorithm was strongly dependent on the use of depressions, in line with findings by Yang et al. (2015). Not using depressions resulted in one connected system flowing out of the deepest depressions towards the ocean, although field observations indicate that water is flowing towards certain depressions. A network consisting of short separate channels was obtained by keeping every pit deeper than 0.01 metres as a true depression. The best result was obtained by manually finding an optimal depth threshold for pits. This manual step would be needed for every other location where this method would be applied. Algorithms that allow for flow towards multiple neighbouring cells were shown to perform better than single directional flow algorithms (Holmgren, 1994). Nevertheless, single directional flow algorithms were often used for studying meltwater features on the Greenland ice sheet (GrIS) and yielded similar results as multi directional flow algorithms (Yang et al. (2015) and King et al. (2016)). For the Nivlisen ice shelf, a single directional flow algorithm generally followed the same flow paths as the A^T algorithm used in this study. The single directional routing network did deviate at some locations from the potential routing network presented at this study, connecting otherwise unconnected flow paths. This observed difference, in contrast to the similarities found in literature, could have been caused by the low slope of the Nivlisen ice shelf of 0.05%, in contrast to the steeper (5 to 16%) glaciers of Greenland (King et al., 2016).

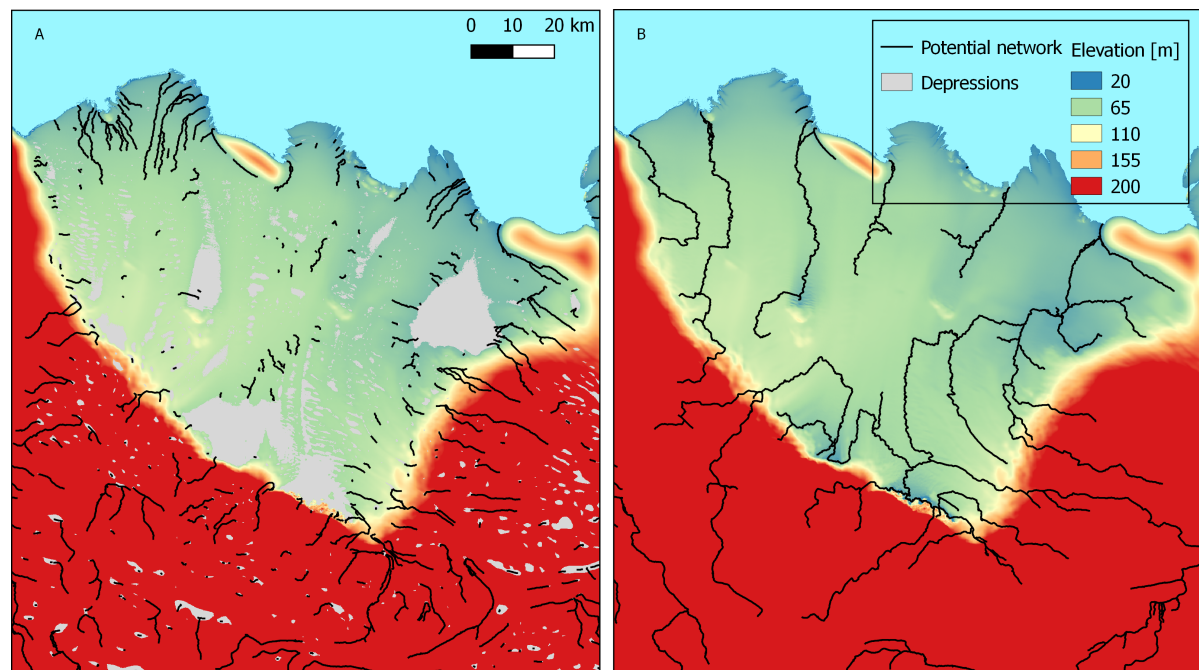


Figure 3.5: A) The result for the routing method, but including every depression into the algorithm instead of depressions only deeper than 9.5 metres. The accumulation threshold is set to 1000 instead of 10.000 to show all the small river segments created. Shorter and separate potential routing channels are created and no real network forms. B) The result for the routing method, but without using any depression. The accumulation threshold is set to 10.000. One large network dominates the ice shelf and connects to the ocean, after passing through some of the deepest points on the Nivlisen ice shelf. These are located close to the grounding line in the south-west and on the east side of the ice shelf.

This section showed the potential for using an automated approach for the creation of a potential routing network (Figure 3.4). The results indicate that the meltwater network will not be able to extend towards the ice shelf cliff and thus would not be able to drain meltwater into the ocean. A deep and large depression present at the current end point of the meltwater network might prevent the network from extending further over the surface of the ice shelf than it does today. Other potential networks on the Nivlisen ice shelf do terminate at the ice cliff and would be able to transport water to the ocean, if surface water would occur in their catchment, as on the Nansen ice shelf (Bell et al., 2017).

Potential routing networks are present over the entire Nivlisen ice shelf, but meltwater features are only observed in the South-East part. To explain why no meltwater networks developed outside this region, climate data is studied in section 3.3.2.

3.3. Climate data / physical drivers

The previous section presented the results from the developed routing method. It was shown that the potential routing network closely matches the shape of the observed meltwater features. Thus the topography has a strong influence on the shape of the meltwater features. The next section presents the analysis of climate data. This data might explain the absence of meltwater features in the north-west part of the Nivlisen ice shelf. Three different steps were executed to find a link between climate data and the meltwater observations. Section 3.3.1 presents the results from correlation calculations between calculated meltwater volumes based on observations and two climate variables. Thereafter, the meltwater and refreeze product from RACMO were integrated over the timesteps as defined by the observations and a water balance was made. Both in time and space, a comparison is made to observed meltwater volumes and areas. The results can be found in section 3.3.2. The third section considers a daily time step and compares the number of days where snowmelt exceeds the refreeze rate to observations of meltwater features (section 3.3.3). Finally, in section 3.3.4, all the results are discussed.

3.3.1. Correlation

The Pearson correlation coefficient (PCC) was calculated between two climate variables and the calculated total volume of meltwater features. The incoming short wave radiation (Figure 3.6.a) and the temperature (Figure 3.6.b) were both extracted from the REMA dataset. Since the calculated meltwater volumes were only available on specific dates (because they were based on satellite observations), the climate data needed to be sampled in the same time frame and interval. Therefore, mean short wave radiation and temperature per timestep were calculated first. For radiation, the PCC was found to be 0.52. For temperature, the PCC was 0.34 (Figure 3.7). Since a PCC of 1 indicates a perfect correlation and a PCC of 0 no correlation at all, a PCC of 0.52 indicates that some correlation did exist between radiation and meltwater volume. The PCC for temperature is a bit lower, which indicated that the correlation is less strong.

Important to realize is the fact that the number of data points used was very low. Only 12 points were compared in the PCC analysis. Therefore, these results are not very robust. A larger dataset, with at least 50 observations, would be needed to reliably tell something about the link between the two climate variables and calculated meltwater volumes. Since incoming short wave radiation is one of the components of the energy balance for surface melt (Bougamont et al., 2005), it was expected to find a stronger correlation between calculated meltwater volume and short wave radiation. Since the PCC does not include any spatial information, both the meltwater and refreeze product of RACMO were used to further study climatic drivers in section 3.3.2. As explained in section 2.4, the meltwater product is based on a full energy balance, which includes short wave radiation.

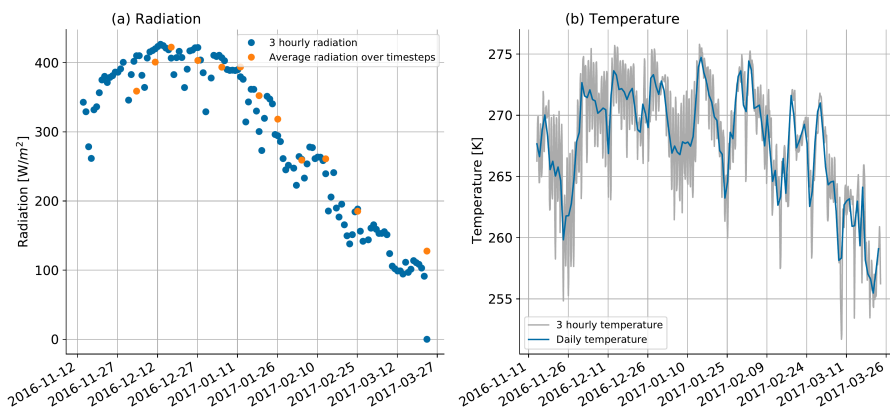


Figure 3.6: (a) Modelled incoming short wave radiation from RACMO for one location in the centre of the Nivlisen ice shelf and (b) modelled temperature from RACMO for one location in the centre of the Nivlisen ice shelf. The modelled short wave radiation showed a clear trend over the season, where the radiation drops when the summer season is ending and the maximum was found during the period (2016-12-12 to 2017-01-11) of largest observed meltwater growth.

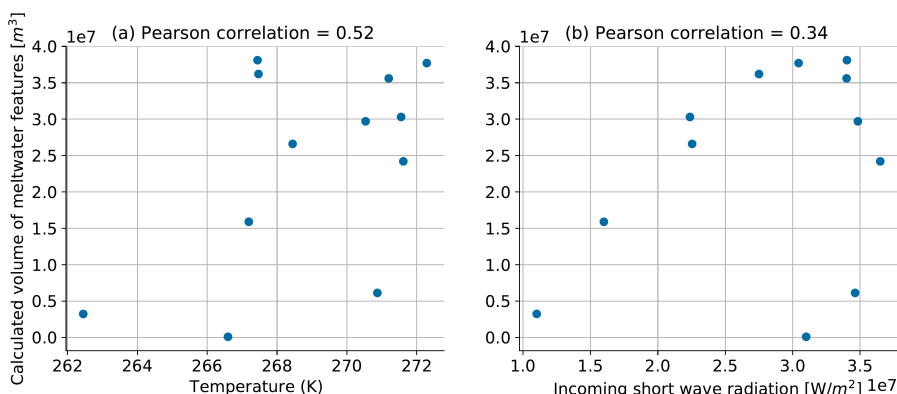


Figure 3.7: Pearson correlation for (a) temperature (PCC = 0.52) and (b) radiation (PCC = 0.34) with the calculated volume of observed meltwater features.

3.3.2. Meltwater production: development during season

The total amount of modelled snowmelt during the melting season was $5.4 \cdot 10^8 \text{ m}^3$. The maximum modelled snowmelt occurred from 2017-01-13 until 2017-01-19, when $1.8 \cdot 10^8 \text{ m}^3$ (33% of the total seasonal snowmelt) modelled snowmelt was produced (Figure 3.8.a). The onset of modelled snowmelt coincided with the first observations of meltwater features on 2016-12-04. The highest modelled snowmelt production occurred at a time when no growth in calculated meltwater volume was observed. Moreover, the large amount of nett modelled meltwater production ($0.6 \cdot 10^7 \text{ m}^3$) at 2017-01-19 (Figure 3.8.b) was not reflected in an increase in calculated volume of the observed meltwater features. In fact, the calculated volume decreased by $0.4 \cdot 10^6 \text{ m}^3$ (Figure 3.2.c). After this timestep, the calculated volume kept decreasing slowly. The modelled snowmelt also declined and dropped to zero before 2017-02-13, after which the remaining observed meltwater features (total volume of $2.7 \cdot 10^7 \text{ m}^3$) shrank further to almost zero in volume during the following month. The nett modelled meltwater production calculated from RACMO data did not match the calculated meltwater volumes of the observed meltwater features during the summer of 2016-2017.

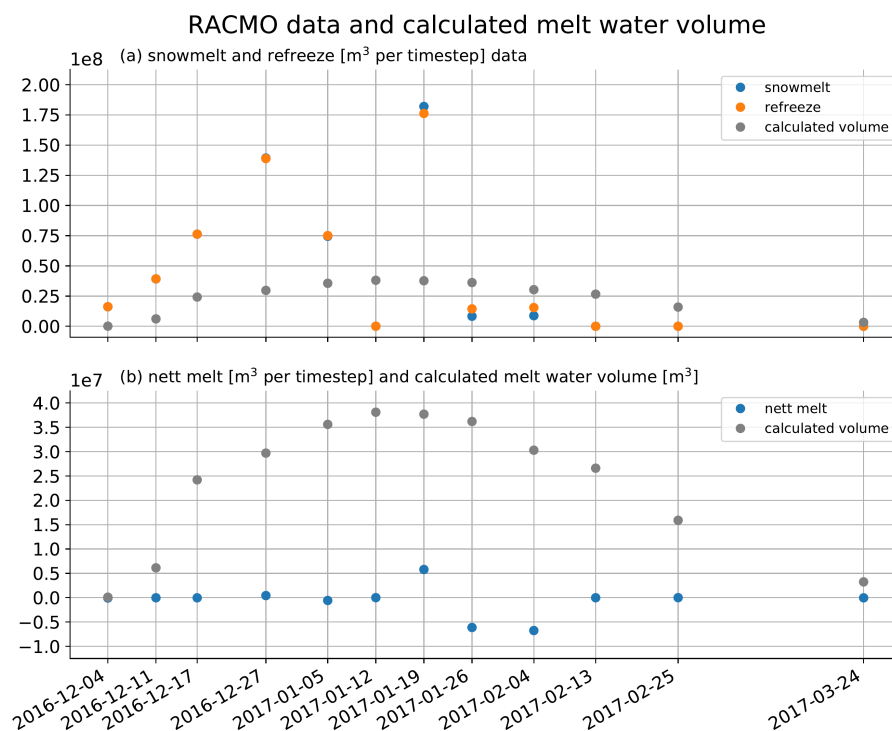


Figure 3.8: (a) Snowmelt and refreezing data as modelled by RACMO, compared with the calculated meltwater volume of the observed meltwater features. (b) The calculated meltwater volume of the observed meltwater features compared with the modelled nett snowmelt production. Although modelled snowmelt alone is large enough to provide the water found in the observed meltwater features, the refreezing during each timestep is almost similar to the modelled snowmelt. This results in a modelled nett meltwater production close to zero.

The modelled refreeze of water was almost equal to the snowmelt, except for the three timesteps of 2017-01-19, 2017-01-26 and 2017-02-04. This resulted in a nett modelled meltwater production value close to zero. The summed nett modelled meltwater production over the entire melting season was $-7.5 \cdot 10^6 \text{ m}^3$, so more water was modelled to be refrozen than melted. A negative nett modelled meltwater production ($-6.1 \cdot 10^6 \text{ m}^3$ and $-6.7 \cdot 10^6 \text{ m}^3$) was found on 2017-01-26 and 2017-02-04, more water was modelled to be refrozen than snow melted. A shrinkage of the calculated volume of the observed meltwater features took place at the same time. The spatial patterns of modelled snowmelt and refreezing are very similar as well. Modelled snowmelt is highest in the south-east part of the Nivlisen ice shelf, close to the grounding line, and almost zero in the north-west (Figure 3.9).

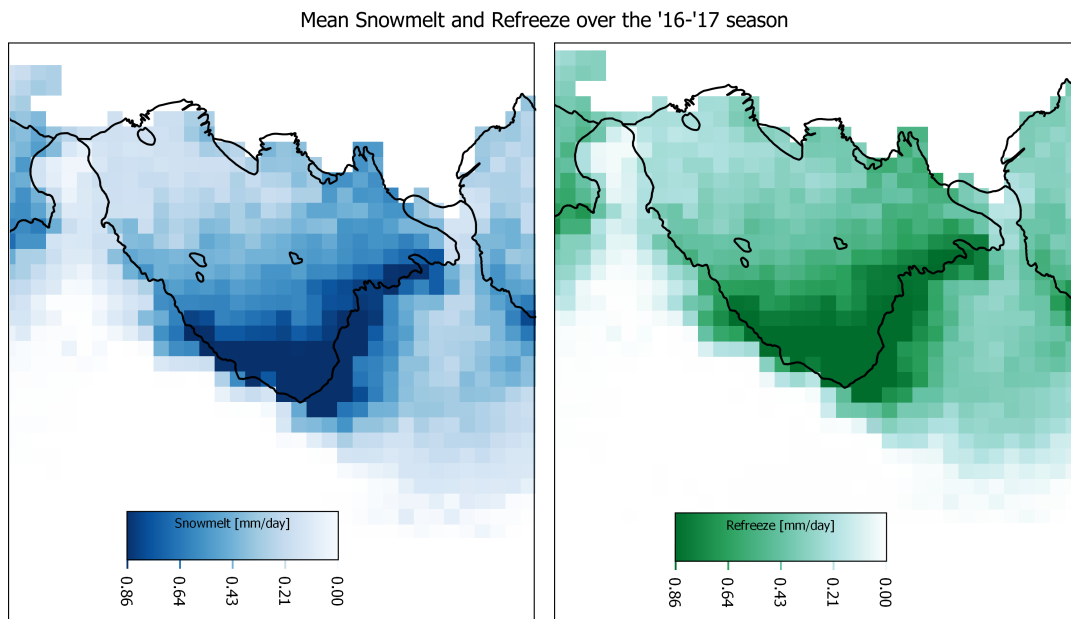


Figure 3.9: Temporal mean modelled snowmelt and refreezing over the 2016-2017 melting season on the Nivlisen ice shelf. Both snowmelt and refreezing are concentrated in the south-east part of the ice shelf, close to the grounding line. Little to no snowmelt is modelled in the north-west region. Patterns of snowmelt and refreeze are very similar.

3.3.3. Daily melt and refreeze

The snowmelt and refreezing products analysed in the previous section were found to be very similar. Almost all water is refrozen in the same timestep as it melted. Therefore, the same data is also studied on a daily resolution. The difference between the modelled snowmelt and refreeze data was zero or very close to zero for the largest part of the summer of 2016-2017 as well (Figure 3.10). The period from 2016-12-04 until 2017-01-05 does have significant modelled meltwater production which matches with the growth of the calculated volume of observed meltwater features. However, the modelled refreezing rate is very similar, resulting in almost no nett modelled melt production. The nett modelled melt production is defined as the modelled snowmelt minus the modelled refreezing during one day. During the period from 2016-12-27 to 2017-01-12, the modelled melt production was mainly zero, whereas the calculated volume of the observed meltwater features was still rising during that time. The nett modelled melt production is (close to) zero for almost the entire period in which a growth in calculated volume of the observed meltwater features was found. Additionally, at the moment a large nett modelled melt production was found, on 2017-01-15, the calculated volume of observed meltwater features was already decreasing (Figure 3.10.b).

The spatial pattern of the number of days where the nett modelled melt production was positive, was studied as well (Figure 3.11). The maximum number of days where the nett modelled melt production was positive, was 12 for any cell within the area of the Nivlisen ice shelf. The area with the most positive nett modelled melt production days is concentrated in the south of the Nivlisen ice shelf, in the same region as the observed meltwater networks.

3.3.4. Discussion

The concentration of meltwater production close to the grounding line is consistent with findings by Lenaerts et al. (2017). The low amount of nett meltwater production was not expected. Observations showed that meltwater features were present on the ice shelf. Even though calculated depths might have been over- or underestimations of the real depth, a large volume of water was present on the surface. Nevertheless the climate data did not support the development of large meltwater features. This is either caused by an underestimation of the snowmelt or an overestimation of the actual refreezing. Previous research ((Lenaerts et al., 2017) and (Lenaerts et al., 2018)) already identified that surface melt is indeed underestimated, especially in the regions close to the grounding lines due to persistent katabatic winds. These winds cause a temperature

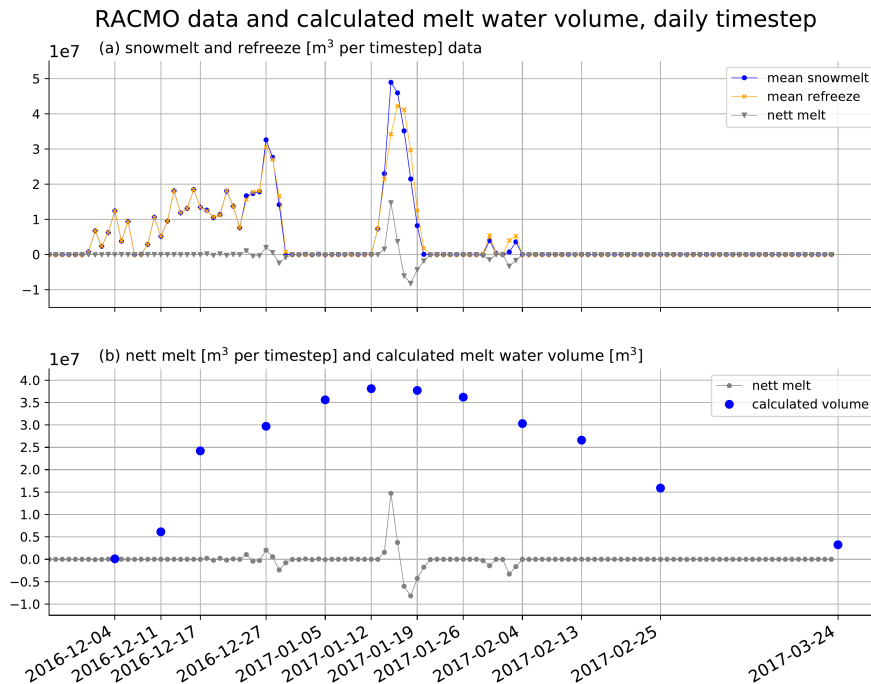


Figure 3.10: (a) Snowmelt and refreezing as modelled by RACMO on a daily time step. The snowmelt and refreezing rate were very similar for the major part of the summer, resulting in a nett melt production close to zero. (b) Calculated melt water surplus on a daily time step compared to calculated meltwater volumes. The calculated meltwater volumes were larger than the modelled nett melt production and a significant nett meltwater production in between 2017-01-12 and 2017-01-19 was not reflected in an increase in calculated meltwater volume of the observed meltwater features.

rise of 3K and surface erosion of the snow layer. Due to the erosion, blue ice areas are exposed. Blue ice has a higher albedo than snow and therefore melt is enhanced in these areas (Lenaerts et al., 2017). Since the amount of water refrozen is partly dependent on the pore space available in the firn layer (see also section 1.4.3) (Bougamont et al., 2005) and the katabatic winds cause the firn layer to become thinner, this could also be an explanation for the overestimation of refreezing. The formation of ice lenses close to the surface is another possible reason for an overestimation of refreezing. Refrozen meltwater in the firn layer prevents meltwater from percolating further and the available pore space is thus decreased (Buzzard et al., 2018). This also limits the refreezing rate and enhances surface lake formation. In comparison, only about 40% of the meltwater refreezes in the firn on Greenland in multiple climate simulations (Van Angelen et al., 2012).

RACMO was not able to quantitatively match the modelled snowmelt and refreeze rates with the increase in calculated melt water feature volumes. This was observed both in the integrated snowmelt/refreeze rate per time step, as in the daily rates. Possibly, this is due to an underestimation of melt and a poor implementation of refreeze calculations within the model (Lenaerts et al., 2017). However, the spatial pattern of days where snowmelt exceeds the refreeze rate, did show that the highest amount of days was found within the area where meltwater features were most abundant (Figure 3.11).

3.4. Roi Baudouin ice shelf

The previous sections explained the results found after studying the climate data and enables this study to answer the third question posed. The meltwater and refreezing product from RACMO was not able to fully explain the total volume of the observed meltwater features. However, the areas with the highest number of days when melting rate exceeded refreeze rate, did overlap with the regions where meltwater features are mainly concentrated. To further support the findings from the previous sections, the Roi Baudouin ice shelf was included in this study. There are three distinct regions on the Roi Baudouin ice shelf where meltwater features are present, of which two are shown in Figure 3.12. Because the manual digitization of meltwater features was very time intensive, it was decided to only focus on the meltwater features in the middle of the Roi Baudouin ice

Number of days where snowmelt exceeds refreeze rate

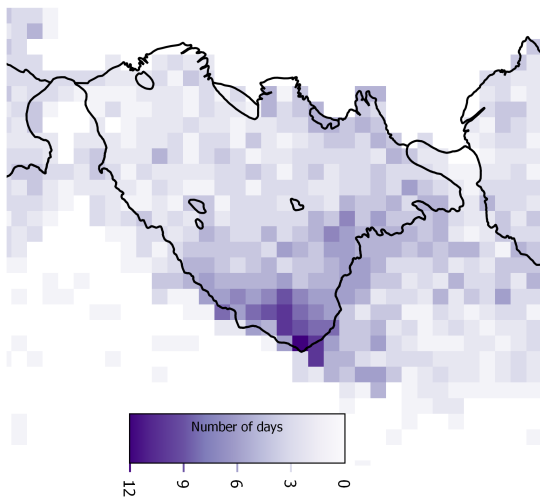


Figure 3.11: Number of days with a positive modelled nett meltwater production. The area where the meltwater features originated during the summer of 2016-2017 has the highest number of nett positive days.

shelf. Besides this, only the maximum extent of the meltwater features has been digitized. By this simplification, the temporal development during the season was not studied for the Roi Baudouin ice shelf. Below, area and volume calculations, results from the routing method and the analysis of climate data are presented.

3.4.1. Area and volume

Three separate meltwater networks developed during the summer of 2016-2017. The maximum extent of one of these melt water networks, occurring on 2017-01-22, was digitized to determine its area: $1.8 \cdot 10^8 \text{ m}^2$. No separate depth calculations were executed for this network. Instead, the mean depth ($\pm 50\%$) found at the Nivlisen ice shelf was taken to calculate a likely range for the total volume of the observed network. The calculated volume was $4.5 \pm 2.2 \cdot 10^7 \text{ m}^3$. The observed meltwater network on the Roi Baudouin had about the same dimensions as the network found on the Nivlisen ice shelf.

3.4.2. Topography and routing

The digitized meltwater features overlapped largely with the created potential routing network (Figure 3.12). At some stretches of meltwater features, the shape of the potential routing network matched very well with the observed meltwater, but is shifted northward. This is probably due to the constant movement of ice, which is discharged from the ice sheet. A large part of the potential routing network did not connect to the ocean, but terminated in deep ($>20 \text{ m}$) depressions close to the grounding line. This was also the location where meltwater features were observed.

3.4.3. Climate data

The RACMO snowmelt and refreezing data were also combined for the Roi Baudouin ice shelf. Temporal patterns were very similar to the climate data from the Nivlisen ice shelf. Refreezement follows snowmelt very closely throughout the season. An average of $0.32 \cdot 10^8 \text{ m}^3$ of snowmelt is produced during the first three timesteps, after which a maximum snowmelt of $1.8 \cdot 10^8 \text{ m}^3$ is produced from 2016-12-17 to 2016-12-27. Only small amounts of meltwater are produced after 2017-01-26. The refreezing was larger than the melt water produced on time steps following the two largest melt events (2017-01-05 and 2017-01-26). The total water balance over the entire melt season was $-2.0 \cdot 10^7 \text{ m}^3$ (Figure 3.13). The spatial pattern showed similarities with the findings from the Nivlisen ice shelf as well. Snowmelt (and refreezement) were largest in the region close to the grounding line. No spatial variation from west to east was found (Figure 3.14). The number of days with a positive nett meltwater production was also calculated and the spatial pattern was similar as found on the Nivlisen ice shelf (Figure 3.15). The locations with the highest amount of days with a positive nett meltwater production were concentrated in the areas where meltwater features were observed.

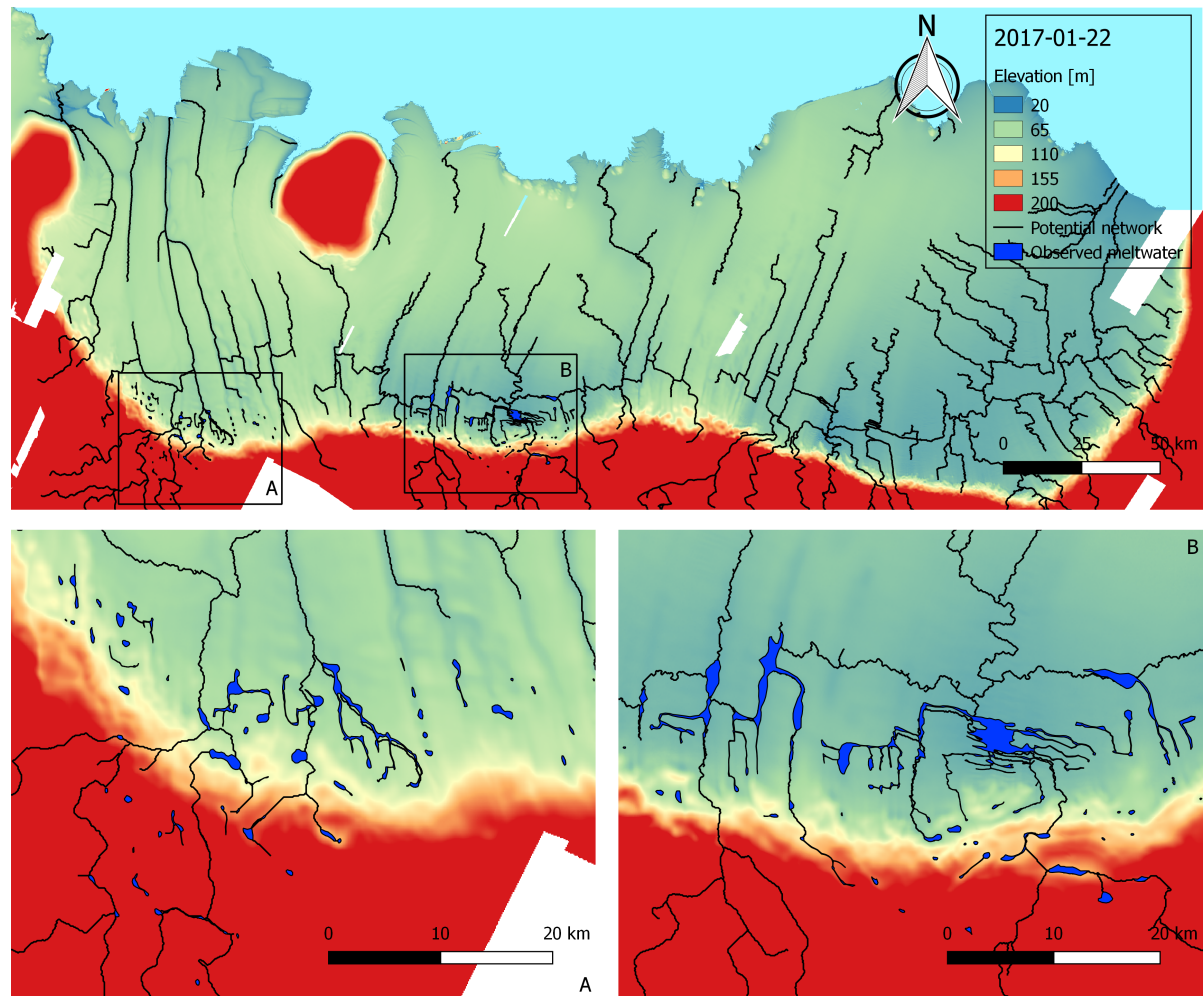


Figure 3.12: Overview of the potential network created with a threshold for accumulation of 10,000 for the Roi Baudouin ice shelf. In subfigure A and B, the left and middle meltwater feature found on the ice shelf are shown. The third meltwater feature present on the Eastern side of this ice shelf is not depicted. The potential routing network matches the shape of the observed meltwater features often, although a northward shift can be observed, especially in subfigure B.

3.4.4. Discussion

The results described above were all very similar to those found at the Nivlisen ice shelf. The routing method created a network overlapping with the observed meltwater features and the climate data showed the same patterns as well. The found location of meltwater features and the concentration of snowmelt close to the grounding line were also supported by Lenaerts et al. (2017). The shift northwards of the observed meltwater features in comparison to the potential routing network was only found on the Roi Baudouin ice shelf, caused by the faster ice flow in comparison to the Nivlisen ice shelf (Rignot et al., 2011). This shows the effect of the movement of the ice shelf. The DEM was made based on satellite imagery from 2014 and 2015 and thus did not incorporate ice sheet flow from that point onwards (Howat et al., 2018). This also leads to errors when using the digital elevation model to calculate depths and volumes of the meltwater features. Since no full analysis of the temporal evolution of the volume of the observed meltwater features was executed, no complete comparison was made between calculated volumes of the observed meltwater features and the modelled (nett) melt production. Similarly to the Nivlisen ice shelf, the modelled nett melt production was close to zero for the largest part of the 2016-2017 summer, caused by the refreeze data matching the snowmelt data very closely.

3.5. General discussion

The previous four sections showed the results for the three topics for the Nivlisen ice shelf and the partial analysis for the Roi Baudouin ice shelf. The area, depth and volume of the meltwater features was calculated and an

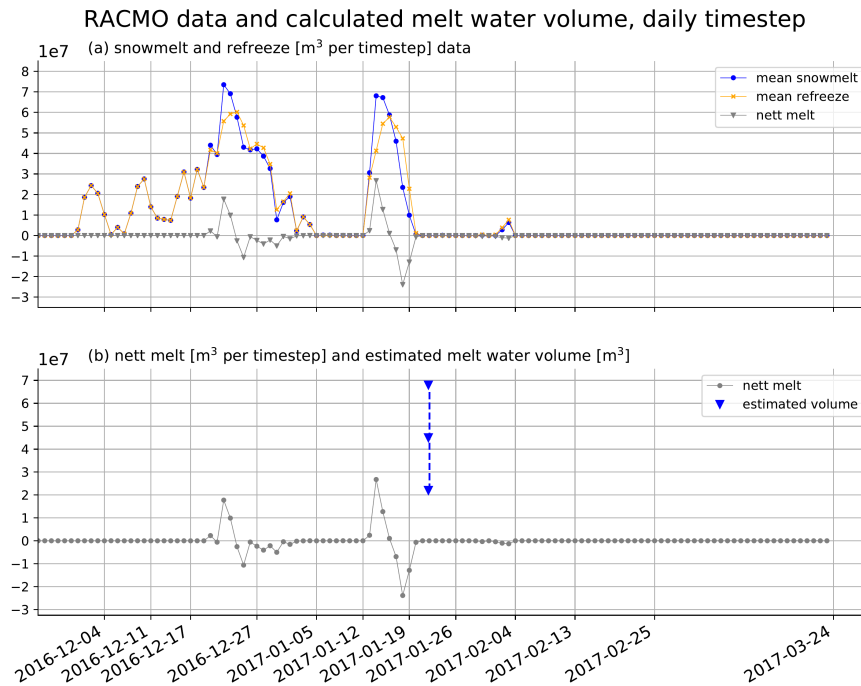


Figure 3.13: (a) Modelled snowmelt, refreezing from RACMO and calculated nett meltwater production data. The snowmelt and refreezing rates are very similar and result in a nett meltwater production which is close to zero for the major part of the summer season. (b) Calculated nett meltwater production compared with the estimated volume on the Roi Baudouin ice shelf on 2017-01-22. The blue triangles depict the estimated range of the possible volume of the meltwater network on the Roi Baudouin ice shelf. No separate depth calculations were executed. Instead, the mean depth found at the Nivlisen ice shelf ($\pm 50\%$) was used to calculate the possible volume at the Roi Baudouin ice shelf.

analysis of the spatial and temporal development was made (section 3.1). A potential routing network was created and showed similarities with the observed meltwater features present on the ice shelf (section 3.2). Climate data was analysed, but was proven to not be able to explain the volume of the meltwater features. However, it was able to give an indication of where meltwater features are likely to develop based on the number of days when meltwater rates exceed melting rates (3.3). Finally, the same analysis was executed for the Roi Baudouin ice shelf. Results found for the Roi Baudouin ice shelf were largely similar to the findings on the Nivlisen ice shelf (section 3.4). With these four results, four general discussion points are presented below.

3.5.1. Calculated volumes in relation with RACMO climate data

The calculated volumes are based on the observations of meltwater area and calculations of mean water depths. The maximum volume stored in the meltwater network found on the Nivlisen ice shelf was about $5 \cdot 10^7$ m³. The research of Dell et al. (2020) supports this finding. The largest calculated nett melt production on one day was $1.5 \cdot 10^7$ m³ and occurred only after the observed meltwater network had reached its maximum volume. Hence this study did not find a quantitative climatological explanation in RACMO for the observed meltwater features. Either an additional water source should have been found, or the RACMO data underestimates snowmelt or overestimates refreeze. Lenaerts et al. (2017) showed that snowmelt is indeed underestimated, but it is uncertain if adapting RACMO to predict higher snowmelts would also cause an increase in refreeze rate. This would mainly depend on the amount of pore space modelled in RACMO (Bougamont et al., 2005). An increase in snowmelt of 20% would be sufficient, if refreeze rate would remain constant, in order to generate enough nett meltwater production to explain the found meltwater volumes. A process that could provide an additional water source is precipitation, also found within RACMO. A first analysis of precipitation data in this study showed that liquid precipitation (precipitation when air temperature is above 2 °C (Oerlemans, 1991)) during the melting season would only contribute a very small amount of water to the total water production by snowmelt. For a large meltwater feature on the Amery ice shelf (also mentioned in section 3.1.4), the total volume of the lake was also compared to RACMO data (Kingslake et al., 2017a). This lake had a similar volume to the amount of water generated in the region surrounding the lake (Kingslake

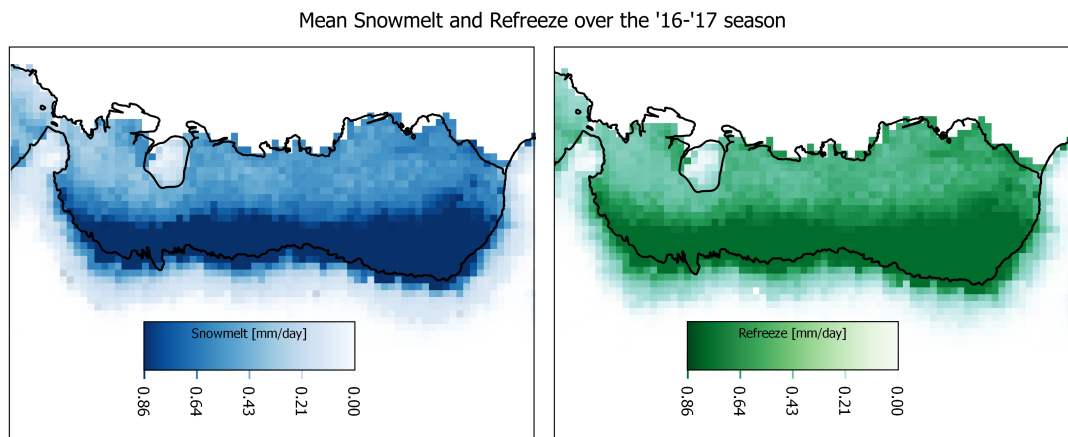


Figure 3.14: Temporal mean snowmelt and refreezing over the 2016-2017 melting season for the Roi Baudouin ice shelf. The temporal pattern of snowmelt and refreeze are very similar and highest close to the grounding line.

Number of days where snowmelt exceeds refreeze rate

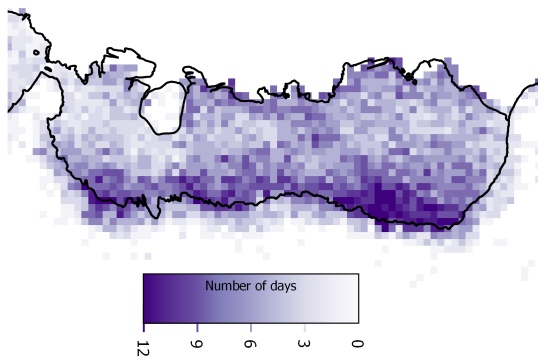


Figure 3.15: Number of days with a modelled nett positive melt production. The areas with the highest number of days are close to the grounding line, in the regions where meltwater features were observed.

et al., 2017b). However, this study did only consider meltwater production and excluded the refreeze data. Moreover, the entire ice shelf was used to calculate the total volume of meltwater produced, instead of the catchment of the lake. The study also suggested to integrate melting rates over individual catchments as was done here (Kingslake et al., 2017b). Nevertheless, the concentration of number of days where a positive nett meltwater production was found, was located in the same region as the observed meltwater features, both for the Nivlisen and Roi Baudouin ice shelf. This demonstrated that the number of days with a positive nett meltwater production is a first indicator of possible locations for meltwater network development.

3.5.2. Future development of the meltwater network

The main features of the observed meltwater systems on the Nivlisen and Roi Baudouin ice shelf in 2016-2017 followed the paths of the potential routing networks. The goal of this study was to present a detailed analysis of one season, since both climate and satellite data were available during the summer of 2016-2017. However, as an extra step, satellite imagery from the summers from 2017 up to 2020 were used to make a multiannual comparison as well. The maximum extent of the meltwater network on the Nivlisen ice shelf progressed further each following year (Figure 3.16). The networks which redeveloped each summer, perfectly followed the lines of the created potential routing network. This highlights the potential of using a flow routing algorithm as presented in this study for predicting likely flowpaths of meltwater features in the future. In 2020 the network terminated in a lake formed on the eastern side of the ice shelf. A large depression is present at this location. Based on REMA, the area was $2.6 \cdot 10^8 \text{ m}^2$ and the average depth was 5 metre. This depression is thus capable of storing roughly $1.3 \cdot 10^9 \text{ m}^3$ of water, 30 times the amount stored in the entire meltwater net-

work in 2016-2017. Therefore, it is not very likely that the observed meltwater network on the Nivlisen ice shelf will drain into the ocean in the near future. Instead, large quantities of water might be stored on one single location. This has potential consequences for the stability of the ice shelf and makes the ice shelf more vulnerable for a potential collapse (Bell et al. (2017) and Bell et al. (2018)).

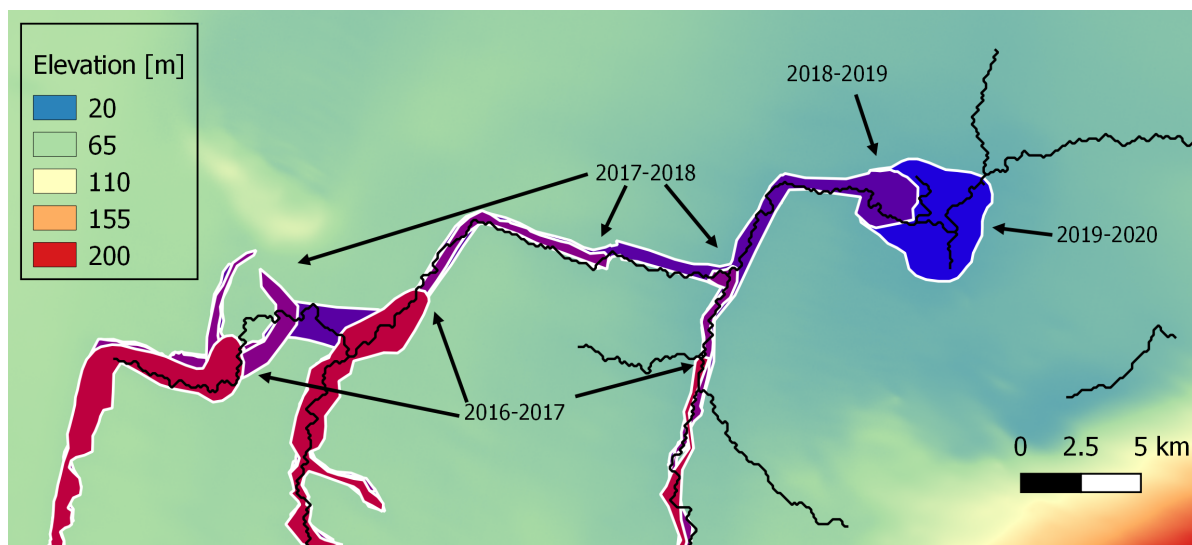


Figure 3.16: Evolution of the three main meltwater features for the summer seasons from 2016-2017 until 2019-2020. The development of the meltwater features follows the potential routing network (black line) created in this study very closely.

3.5.3. Role of firn air content

As previously discussed in section 3.3.4, the pore space in the firn layer (the firn air content) plays an important role in storing and refreezing meltwater. Only after the drainage capacity of the firn layer is lower than the snowmelt rate, water starts to pond on the surface (Kuipers Munneke et al., 2014). Both the Nivlisen and Roi Baudouin ice shelf have a relative low firn air content (Kuipers Munneke et al., 2014). It is projected that the firn air content will decrease further over the 21st and 22nd century (Ligtenberg et al., 2014), increasing the potential for surface ponding. Alley et al. (2018) combines radar backscatter properties depending on the saturation of firn layers with the number of melt days in a summer season and ice shelf geometry to derive a vulnerability index to hydrofracturing. The area with observed meltwater features is found to be less vulnerable than areas closer to the ice cliff (Alley et al., 2018). However, it was expected that the firn air content is considerably lower close to the grounding line, since meltwater features are only able to develop in that region.

3.5.4. Influence of climate change

It is projected that the surface melt on Antarctica will double towards the end of the 21st century (Pattyn et al., 2018). Due to a combination of a drop in firn air content (Ligtenberg et al., 2014) and the possible formation of ice lenses in the firn layer (Buzzard et al., 2018), it was expected that the refreezing rate will simultaneously drop as well. Climate models showed that firn air content is indeed dropping under climate scenario A1B (a rapid economic growth while using both fossil and renewable fuels) (Kuipers Munneke et al. (2014) and Ligtenberg et al. (2014)). With the firn air content dropping and the surface melt rising, a large increase in net meltwater production could be expected, probably causing a rise in the extent of meltwater features on the ice shelf. Since a large depression was identified as the endpoint of the current meltwater network during the routing analysis, this additional water is likely to be stored on the ice shelf. This surface ponding would cause the ice shelf to become more sensitive to hydrofracturing and would thus weaken the ice shelf significantly (Banwell and MacAyeal, 2015).

4

Conclusions and recommendations

Based on the results found in Chapter 3, the conclusions were made and are presented below in section 4.1. This report ends with recommendations for extensions to and new studies on the same topic as this study (section 4.2).

4.1. Conclusions

This study has combined satellite imagery, a digital elevation model and climate data to analyse the detailed development of meltwater networks during one melting season on the Nivlisen ice shelf. The findings were further supported by an additional partial analysis of the Roi Baudouin ice shelf. Below, each question is repeated and answered, supported by the results presented in Chapter 3.

What is the temporal and spatial development of meltwater networks during one melting season?

By manually delineating meltwater features as seen in optical satellite imagery, the temporal and spatial development of meltwater networks on the Nivlisen ice shelf was analysed for the melting season of 2016-2017. While in the beginning of the melting season meltwater features were mostly separate lakes, this evolved in a connected system slowly expanding northwards, ending 40 kilometres from the grounding line and 50 kilometres from the ice shelf cliff. Meltwater features were observed on the Nivlisen ice shelf from 2016-12-04 until 2017-03-24 and the maximum extent was on 2017-01-19. The movement of the front of the system was very slow, indicating that the front is not a freely flowing water mass. A digital elevation model was used to determine the mean depth and total volume of the meltwater network. No significant change in mean depth was found during the melting season. An increase in volume of the meltwater network was predominantly determined by an increase in area. The calculated volumes were in line with the volumes derived by Dell et al. (2020).

Is the topography of an ice shelf a driver for the shape and extent of a meltwater network?

A semi-automated method to create a potential routing network on an Antarctic ice shelf was developed. This method is based on the A^T least cost path algorithm, but extends this further by incorporating real depressions and further automating the procedure to obtain a routing network. Keeping real depressions as endpoint for the routing method was crucial for obtaining a realistic potential routing network. Main branches of the observed meltwater network did often coincide with the potential network branches. To validate the proposed method, it was applied on the Roi Baudouin ice shelf. The potential routing network created matched the observed meltwater features very well on the Roi Baudouin ice shelf. It can be concluded that the routing method developed in this study can also be applied to other ice shelves. Although potential networks are present throughout the entire ice shelf, no meltwater networks are observed outside the South-West region of the Nivlisen ice shelf. Based on these results, this study concludes that the topography of the ice shelf is indeed a driver for the shape and extent of the meltwater network, but does not determine the creation of a network. Other factors should be taken into account as well. The extent of a meltwater network can be limited by the topography, when large depressions are present in the possible flow path.

Is it possible to identify underlying physical drivers of the creation of meltwater networks using available climate data?

Snowmelt and refreezing data from the Regional Atmospheric Climate Model (RACMO) were analysed for the Nivlisen and Roi Baudouin ice shelf. The observed meltwater features developed in the regions with the

highest snowmelt. The amount of water refrozen was very close to the meltwater produced. Therefore the calculated melt water surplus is very low and often close to zero. Too little melt water generation is modelled to account for the amount of water found in the meltwater networks. Hence the snowmelt and refreezing data from the current RACMO model could not be used to further explain the development of the observed meltwater features quantitatively. It is very important that this underestimation of snowmelt or overestimation of refreezing rate is addressed, to be able to further study the hydrological processes on the ice shelves of Antarctica. Nevertheless, it can be concluded from this study that the number of days on which the snowmelt rate exceeded the refreezing rate could be used as a first indication of the locations where the development of melt water features is likely to occur. Regions with more of these days coincided with the parts of the Nivlisen and Roi Baudouin ice shelf where melt water features were present.

4.2. Recommendations

4.2.1. Closing the water balance

This study used snowmelt and refreezing to calculate the net surplus of water. Results in section 3.3.2 showed that an additional water source is needed in order to explain the observed meltwater volumes. Creating a full water balance, including precipitation and other variables from RACMO, might give a net surplus of water that better matches the observed volume, even though uncertainties in RACMO are present. Precipitation alone was not enough to account for the deficit of water when integrating snowmelt and refreezing over the melting season, and certainly did not generate enough water volume to explain the water volume present in the observed melt water features. It is recommended to create a full water balance, although it is also likely that the representation of snowmelt and refreeze rate in RACMO needs to be improved before the water balance can be properly closed.

4.2.2. RACMO constrained by observed meltwater volume

As mentioned in section 3.3.4, the climate data from RACMO underestimates the snowmelt produced severely (Lenaerts et al., 2017). The total nett modelled meltwater production during the season did not match the calculated volume of the meltwater features. Moreover, also the timing of meltwater production did not match the timing of the growth of observed meltwater features. To further improve RACMO, an estimate of the observed meltwater volume can be used to constrain the model during its calibration. Meltwater observations and calculations of the volume stored in the meltwater features are able to serve as a first indication for the minimum amount of nett meltwater production that RACMO should model.

4.2.3. Study firn air content

The firn air content is an indicator for the possibility of meltwater ponding (Kuipers Munneke et al., 2014). It might be worthwhile to study the current firn air content and the projected evolution to be able to better define possible locations where meltwater networks might form and to explain the formation of current networks. Firn air content products with a 5.5 kilometre resolution were used to study the impact of katabatic winds on the melt water production on Antarctica (Lenaerts et al., 2017). It is recommended to combine this data set with melt water observations which can tell us more about the importance of firn air content in relation to the development of meltwater features.

4.2.4. Routing on multiple ice shelves

This study created a potential routing network for two ice shelves. The routing method could be used on multiple ice shelves across Antarctica to study the potential paths meltwater features might take in the future under an increase in melting rates. This would give indications on the ability of ice shelves to discharge water in the ocean. Combining this with projections for melting rates, firn air content and basal melting could provide information about the vulnerability to break up of the ice shelves under projected climate change. GMSL rise projections could be further refined by knowing which ice shelves are more likely to collapse. To use the proposed method on other ice shelves, it is very important that depressions on the ice shelves are dealt with appropriately.

4.2.5. Radar satellites

Using optical satellite imagery to detect meltwater features only works on cloud free days. Sufficient cloud free images were available for the Nivlisen ice shelf in 2016-2017 to follow the development of the meltwater

network. Different locations or different years might have more clouds, limiting the number of observations. Radar satellites are able to overcome this problem and could thus increase the frequency of observations (Miles et al., 2017). Moreover, the radar waves are able to penetrate the upper firn, snow or ice layer. Hence radar satellites do detect supraglacial lakes that are (partly) frozen over and buried subglacial lakes (Miles et al., 2017). The start of operation of Sentinel 1 in 2016 provides a product that has both a high spatial resolution (25 metres) and a relative high temporal resolution (6 days), making this satellite very promising for further research (Miles et al. (2017) and Arthur et al. (2020)). However, it is not always straightforward to distinguish water from ice or slush regions due to the backscattering properties of each medium (Cooley and Pavelsky (2016) and Unterschultz et al. (2009))

Bibliography

- Alley, K. E., Scambos, T. A., Miller, J. Z., Long, D. G., and MacFerrin, M. Quantifying vulnerability of Antarctic ice shelves to hydrofracture using microwave scattering properties. *Remote Sensing of Environment*, 210 (June 2017):297–306, 2018. ISSN 0034-4257. doi: 10.1016/j.rse.2018.03.025.
- Arthur, J. F., Stokes, C., Jamieson, S. S., Carr, J. R., and Leeson, A. A. Recent understanding of Antarctic supraglacial lakes using satellite remote sensing. *Progress in Physical Geography*, page 030913332091611, may 2020. ISSN 03091333. doi: 10.1177/0309133320916114.
- Banwell, A. F. and MacAyeal, D. R. Ice-shelf fracture due to viscoelastic flexure stress induced by fill/drain cycles of supraglacial lakes. *Antarctic Science*, 27(6):587–597, 2015. ISSN 13652079. doi: 10.1017/S0954102015000292.
- Banwell, A. F., MacAyeal, D. R., and Sergienko, O. V. Breakup of the Larsen B Ice Shelf triggered by chain reaction drainage of supraglacial lakes. *Geophysical Research Letters*, 40(22):5872–5876, 2013. ISSN 00948276. doi: 10.1002/2013GL057694.
- Banwell, A. F., Caballero, M., Arnold, N. S., Glasser, N. F., Cathles, L. M., et al. Supraglacial lakes on the {Larsen} {B} ice shelf, {Antarctica}, and at {Paakitsoq}, {West} {Greenland}: a comparative study. *Annals of Glaciology*, 55(66):1–8, 2014. ISSN 0260-3055, 1727-5644. doi: 10.3189/2014AoG66A049.
- Bell, R. E., Chu, W., Kingslake, J., Das, I., Tedesco, M., et al. Antarctic ice shelf potentially stabilized by export of meltwater in surface river. *Nature*, 544(7650):344–348, 2017. ISSN 14764687. doi: 10.1038/nature22048.
- Bell, R. E., Banwell, A. F., Trusel, L. D., and Kingslake, J. Antarctic surface hydrology and impacts on ice-sheet mass balance. *Nature Climate Change*, 2018. ISSN 1758-678X. doi: 10.1038/s41558-018-0326-3.
- Bougamont, M., Bamber, J. L., and Greuell, W. A surface mass balance model for the Greenland Ice Sheet. *Journal of Geophysical Research: Earth Surface*, 110(4), dec 2005. ISSN 21699011. doi: 10.1029/2005JF000348.
- Buzzard, S. C., Feltham, D. L., and Flocco, D. A Mathematical Model of Melt Lake Development on an Ice Shelf. *Journal of Advances in Modeling Earth Systems*, 10(2):262–283, feb 2018. ISSN 1942-2466. doi: 10.1002/2017MS001155.
- Buzzard, S. and Robel, A. A 3D Model of Antarctic Ice Shelf Surface Hydrology. In *AGU Fall Meeting Abstracts*, volume 2019, pages C11A–01, dec 2019.
- Cooley, S. W. and Pavelsky, T. M. Spatial and temporal patterns in Arctic river ice breakup revealed by automated ice detection from MODIS imagery. *Remote Sensing of Environment*, 175:310–322, mar 2016. ISSN 00344257. doi: 10.1016/j.rse.2016.01.004.
- Deconto, R. M. and Pollard, D. Contribution of Antarctica to past and future sea-level rise. *Nature*, 531(7596): 591–597, 2016. ISSN 14764687. doi: 10.1038/nature17145.
- Dell, R., Arnold, N., Willis, I., Banwell, A., Williamson, A., et al. Lateral meltwater transfer across an Antarctic ice shelf. *The Cryosphere*, 14(7):2313–2330, 2020. ISSN 19940424. doi: 10.5194/tc-14-2313-2020.
- Dupont, T. K. and Alley, R. B. Assessment of the importance of ice-shelf buttressing to ice-sheet flow. *Geophysical Research Letters*, 32(4):1–4, feb 2005. ISSN 00948276. doi: 10.1029/2004GL022024.
- Ehlschlaeger, C. Using the AT Search Algorithm to Develop Hydrologic Models from Digital Elevation Data. *Proceedings of International Geographic Information Systems (IGIS) Symposium'89*, (August):275–281, 1989.
- Ettema, J., Van Den Broeke, M. R., Van Meijgaard, E., Van De Berg, W. J., Box, J. E., et al. Climate of the Greenland ice sheet using a high-resolution climate model - Part 1: Evaluation. *Cryosphere*, 4(4):511–527, 2010. ISSN 19940416. doi: 10.5194/tc-4-511-2010.

- Fretwell, P., Pritchard, H. D., Vaughan, D. G., Bamber, J. L., Barrand, N. E., et al. Bedmap2: Improved ice bed, surface and thickness datasets for Antarctica. *Cryosphere*, 7(1):375–393, 2013. ISSN 19940416. doi: 10.5194/tc-7-375-2013.
- Fürst, J. J., Durand, G., Gillet-Chaulet, F., Tavard, L., Rankl, M., et al. The safety band of Antarctic ice shelves. *Nature Climate Change*, 6(5):479–482, 2016. ISSN 17586798. doi: 10.1038/nclimate2912.
- Gleason, C. J., Smith, L. C., Chu, V. W., Legleiter, C. J., Pitcher, L. H., et al. Characterizing supraglacial meltwater channel hydraulics on the Greenland Ice Sheet from in situ observations. *Earth Surface Processes and Landforms*, 41(14):2111–2122, 2016. ISSN 10969837. doi: 10.1002/esp.3977.
- Goldberg, D. N. Ice Shelf Buttressing. *International Encyclopedia of Geography: People, the Earth, Environment and Technology*, pages 1–9, 2017. doi: 10.1002/9781118786352.wbieg0567.
- GRASS Development team. r.fill.dir - GRASS GIS manual, 2020. URL <https://grass.osgeo.org/grass78/manuals/r.fill.dir.html>.
- Holmgren, P. Multiple flow direction algorithms for runoff modelling in grid based elevation models: An empirical evaluation. *Hydrological Processes*, 8(4):327–334, jul 1994. ISSN 08856087. doi: 10.1002/hyp.3360080405.
- Horwath, M., Dietrich, R., Baessler, M., Nixdorf, U., Steinhage, D., et al. Nivlisen, an Antarctic ice shelf in Dronning Maud Land: Geodetic-glaciological results from a combined analysis of ice thickness, ice surface height and ice-flow observations. *Journal of Glaciology*, 52(176):17–30, 2006. ISSN 00221430. doi: 10.3189/172756506781828953.
- Howat, I., Morin, P., Porter, C., and Noh, M.-J. The Reference Elevation Model of Antarctica, V1. *The Cryosphere*, 13(September 2018):665–674, 2018. doi: <https://doi.org/10.7910/DVN/SAIK8B>.
- Keefer, B. J. Effect of Manual Digitizing Error on the Accuracy and Precision of Polygon Area and Line Length. Technical report, nov 1988.
- King, L., Hassan, M. A., Yang, K., and Flowers, G. Flow routing for delineating supraglacial meltwater channel networks. *Remote Sensing*, 8(12):1–21, 2016. ISSN 20724292. doi: 10.3390/rs8120988.
- Kingslake, J., Ely, J. C., Das, I., and Bell, R. E. Widespread movement of meltwater onto and across Antarctic ice shelves. *Nature*, 544(7650):349–352, 2017a. ISSN 14764687. doi: 10.1038/nature22049.
- Kingslake, J., Ely, J. C., Das, I., and Bell, R. E. Corrigendum: Widespread movement of meltwater onto and across Antarctic ice shelves (Nature (2017) 544 (349-352) DOI: 10.1038/nature22049), nov 2017b. ISSN 14764687.
- Kinner, D., Mitasova, H., Stallard, R., Harmon, R. S., and Toma, L. GIS-Based Stream Network Analysis for the Upper Río Chagres Basin, Panama. *The Río Chagres, Panama*, pages 83–95, 2005. doi: 10.1007/1-4020-3297-8_6.
- Kuipers Munneke, P., Ligtenberg, S. R., Van Den Broeke, M. R., and Vaughan, D. G. Firn air depletion as a precursor of Antarctic ice-shelf collapse. *Journal of Glaciology*, 60(220):205–214, 2014. ISSN 00221430. doi: 10.3189/2014JoG13J183.
- Langley, E. S., Leeson, A. A., Stokes, C. R., and Jamieson, S. S. Seasonal evolution of supraglacial lakes on an East Antarctic outlet glacier. *Geophysical Research Letters*, 43(16):8563–8571, 2016. ISSN 19448007. doi: 10.1002/2016GL069511.
- Lea, J. M. The Google Earth Engine Digitisation Tool (GEEDiT) and the Margin change Quantification Tool (MaQiT) — simple tools for the rapid mapping and quantification of changing Earth surface margins. *Earth Surface Dynamics*, 6(3):551–561, jul 2018. ISSN 2196-632X. doi: 10.5194/esurf-6-551-2018.
- Lenaerts, J. T., Lhermitte, S., Drews, R., Ligtenberg, S. R., Berger, S., et al. Meltwater produced by wind-albedo interaction stored in an East Antarctic ice shelf. *Nature Climate Change*, 7(1):58–62, 2017. ISSN 17586798. doi: 10.1038/nclimate3180.

- Lenaerts, J. and Lhermitte, S. Meltwater on an East Antarctic ice shelf, 2016. URL <http://tudelft.pageflow.io/benemelt{#}74887>.
- Lenaerts, J. T., Ligtenberg, S. R., Medley, B., Van De Berg, W. J., Konrad, H., et al. Climate and surface mass balance of coastal West Antarctica resolved by regional climate modelling. *Annals of Glaciology*, 59(76pt1): 29–41, 2018. ISSN 02603055. doi: 10.1017/aog.2017.42.
- Ligtenberg, S. R., Helsen, M. M., and Van Den Broeke, M. R. An improved semi-empirical model for the densification of Antarctic firn. *Cryosphere*, 5(4):809–819, 2011. ISSN 19940416. doi: 10.5194/tc-5-809-2011.
- Ligtenberg, S. R., Kuipers Munneke, P., and Van Den Broeke, M. R. Present and future variations in Antarctic firn air content. *Cryosphere*, 8(5):1711–1723, sep 2014. ISSN 19940424. doi: 10.5194/tc-8-1711-2014.
- Manning, R. On the flow of water in open channels and pipes. *Trans. Inst. Civil Eng. Ireland*, 20:161–207, 1891.
- Marston, R. A. Supraglacial Stream Dynamics on the Juneau Icefield. *Annals of the Association of American Geographers*, 73(4):597–608, 1983. ISSN 14678306. doi: 10.1111/j.1467-8306.1983.tb01861.x.
- Meredith, M., Sommerkorn, M., Cassotta, S., Derksen, C., Ekaykin, A., et al. Polar Regions. In: IPCC Special Report on the Ocean and Cryosphere in a Changing Climate [H.-O. Pörtner, D.C. Roberts, V. Masson-Delmotte, P. Zhai, M. Tignor, E. Poloczanska, K. Mintenbeck, A. Alegria, M. Nicolai, A. Okem, J. Petzold, B. Rama, N.M. Weyer (eds.)]. In press. Technical report, 2019.
- Metz, M., Mitasova, H., and Harmon, R. S. Efficient extraction of drainage networks from massive, radar-based elevation models with least cost path search. *Hydrology and Earth System Sciences*, 15(2):667–678, feb 2011. ISSN 1607-7938. doi: 10.5194/hess-15-667-2011.
- Miles, K. E., Willis, I. C., Benedek, C. L., Williamson, A. G., and Tedesco, M. Toward monitoring surface and subsurface lakes on the Greenland ice sheet using sentinel-1 SAR and landsat-8 OLI imagery. *Frontiers in Earth Science*, 5:58, jul 2017. ISSN 22966463. doi: 10.3389/feart.2017.00058.
- Moussavi, M., Pope, A., Halberstadt, A. R. W., Trusel, L. D., Cioffi, L., et al. Antarctic supraglacial lake detection using landsat 8 and sentinel-2 imagery: Towards continental generation of lake volumes. *Remote Sensing*, 12(1):134, jan 2020. ISSN 20724292. doi: 10.3390/RS12010134.
- Nyberg, B., Buckley, S. J., Howell, J. A., and Nanson, R. A. Geometric attribute and shape characterization of modern depositional elements: A quantitative GIS method for empirical analysis. *Computers and Geosciences*, 82:191–204, 2015. ISSN 00983004. doi: 10.1016/j.cageo.2015.06.003.
- O’Callaghan, J. F. and Mark, D. M. The extraction of drainage networks from digital elevation data. *Computer Vision, Graphics, & Image Processing*, 28(3):323–344, dec 1984. ISSN 0734189X. doi: 10.1016/S0734-189X(84)80011-0.
- Oerlemans, J. A model for the surface balance of ice masses: Part I: alpine glaciers. *Zeitschrift für Gletscherkunde und Glazialgeologie*, 27:63–83, 1991. ISSN 0044-2836.
- Oppenheimer, M., Glavovic, B., J. Hinkel, R. v. d. W., Magnan, A., Abd-Elgawad, A., et al. Sea Level Rise and Implications for Low-Lying Islands, Coasts and Communities. In: IPCC Special Report on the Ocean and Cryosphere in a Changing Climate [H.-O. Portner, D.C. Roberts, V. Masson-Delmotte, P. Zhai, M. Tignor, E. Poloczanska, K. Mintenbeck, A. Alegria, M. Nicolai, A. Okem, J. Petzold, B. Rama, N.M. Weyer (eds.)]. In press. Technical report, 2019.
- Paolo, F. S., Fricker, H. A., and Padman, L. Volume loss from Antarctic ice shelves is accelerating. *Science*, 348(6232):327–331, apr 2015. ISSN 10959203. doi: 10.1126/science.aaa0940.
- Pattyn, F., Ritz, C., Hanna, E., Asay-Davis, X., DeConto, R., et al. The Greenland and Antarctic ice sheets under 1.5 °C global warming, 2018. ISSN 17586798.
- Pritchard, H. D., Ligtenberg, S. R., Fricker, H. A., Vaughan, D. G., Van Den Broeke, M. R., et al. Antarctic ice-sheet loss driven by basal melting of ice shelves. *Nature*, 484(7395):502–505, 2012. ISSN 00280836. doi: 10.1038/nature10968.

- Reese, R., Gudmundsson, G. H., Levermann, A., and Winkelmann, R. The far reach of ice-shelf thinning in Antarctica. *Nature Climate Change*, 8(1):53–57, 2018. ISSN 17586798. doi: 10.1038/s41558-017-0020-x.
- Rignot, E., Mouginot, J., and Scheuchl, B. Ice flow of the antarctic ice sheet. *Science*, 333(6048):1427–1430, sep 2011. ISSN 00368075. doi: 10.1126/science.1208336.
- Rignot, E., Jacobs, S., Mouginot, J., and Scheuchl, B. Ice-shelf melting around antarctica. *Science*, 341(6143): 266–270, 2013. ISSN 10959203. doi: 10.1126/science.1235798.
- Scambos, T. A., Hulbe, C., Fahnestock, M., and Bohlander, J. The link between climate warming and break-up of ice shelves in the Antarctic Peninsula. *Journal of Glaciology*, 46(154):516–530, 2000. ISSN 00221430. doi: 10.3189/172756500781833043.
- Sneed, W. A. and Hamilton, G. S. Evolution of melt pond volume on the surface of the Greenland Ice Sheet. *Geophysical Research Letters*, 34(3):L03501, feb 2007. ISSN 00948276. doi: 10.1029/2006GL028697.
- Stokes, C. R., Sanderson, J. E., Miles, B. W., Jamieson, S. S., and Leeson, A. A. Widespread distribution of supraglacial lakes around the margin of the East Antarctic Ice Sheet. *Scientific Reports*, 9(1), 2019. ISSN 20452322. doi: 10.1038/s41598-019-50343-5.
- Tedesco, M., Lthje, M., Steffen, K., Steiner, N., Fettweis, X., et al. Measurement and modeling of ablation of the bottom of supraglacial lakes in western Greenland. *Geophysical Research Letters*, 39(2):n/a–n/a, jan 2012. ISSN 00948276. doi: 10.1029/2011GL049882.
- Trusel, L. D., Frey, K. E., Das, S. B., Karnauskas, K. B., Munneke, P. K., et al. Divergent trajectories of Antarctic surface melt under two twenty-first-century climate scenarios. *Nature geoscience*, 8(December), 2015. doi: 10.1038/NCEO2563.
- Unterschultz, K. D., van der Sanden, J., and Hicks, F. E. Potential of RADARSAT-1 for the monitoring of river ice: Results of a case study on the Athabasca River at Fort McMurray, Canada. *Cold Regions Science and Technology*, 55(2):238–248, feb 2009. ISSN 0165232X. doi: 10.1016/j.coldregions.2008.02.003.
- Van Angelen, J. H., Lenaerts, J. T., Lhermitte, S., Fettweis, X., Kuipers Munneke, P., et al. Sensitivity of Greenland Ice Sheet surface mass balance to surface albedo parameterization: A study with a regional climate model. *Cryosphere*, 6(5):1175–1186, 2012. ISSN 19940416. doi: 10.5194/tc-6-1175-2012.
- van Wessem, J. M., van de Berg, W. J., Noël, B. P. Y., van Meijgaard, E., Amory, C., et al. Modelling the climate and surface mass balance of polar ice sheets using RACMO2 – Part 2: Antarctica (1979–2016). *The Cryosphere*, 12(4):1479–1498, apr 2018. ISSN 1994-0424. doi: 10.5194/tc-12-1479-2018.
- Yang, K. and Smith, L. C. Supraglacial streams on the greenland ice sheet delineated from combined spectral-shape information in high-resolution satellite imagery. *IEEE Geoscience and Remote Sensing Letters*, 10(4): 801–805, 2013. ISSN 1545598X. doi: 10.1109/LGRS.2012.2224316.
- Yang, K., Smith, L. C., Chu, V. W., Gleason, C. J., and Li, M. A Caution on the Use of Surface Digital Elevation Models to Simulate Supraglacial Hydrology of the Greenland Ice Sheet. *IEEE Journal of Selected Topics in Applied Earth Observations and Remote Sensing*, 8(11):5212–5224, nov 2015. ISSN 1939-1404. doi: 10.1109/JSTARS.2015.2483483.
- Yang, K., Smith, L. C., Chu, V. W., Pitcher, L. H., Gleason, C. J., et al. Fluvial morphometry of supraglacial river networks on the Southwest Greenland ice sheet. *GIScience and Remote Sensing*, 53(4):459–482, jul 2016. ISSN 15481603. doi: 10.1080/15481603.2016.1162345.

A

Appendix A

A.1. Glossary

<i>Austral summer</i>	The summer season on the Southern hemisphere and on Antarctica specifically. From November to March.
<i>DEM</i>	A digital elevation model. A representation of the elevation of the terrain in a grid consisting of cells. Each cell has an assigned elevation.
<i>Endorheic lake</i>	A lake that does not have an outflow point.
<i>Exorheic lake</i>	A lake that does have an outflow point.
<i>Firn</i>	A mixture of snow and ice. Contains pores where water can infiltrate.
<i>Grounding line</i>	Line where the ice sheet (grounded on the bedrock layer) starts to float and thus becomes an ice shelf.
<i>Ice shelf</i>	The ice on Antarctica that rests on the bedrock layer.
<i>Ice sheet</i>	The ice on Antarctica, attached to the main land, that floats on the ocean.
<i>Katabatic winds</i>	Winds coming from the high elevation inland of Antarctica, blowing down towards the coastal areas. These winds warm up during their descend and can cause an increase in temperature of 3 °C (Lenaerts et al., 2017).
<i>Moulin</i>	A vertical shaft in the firn or ice layer in which surface water drains and the start of a tunnel through which water flows.
<i>Nunatak</i>	Exposed bedrock formations on the Antarctic ice sheet.
<i>Supraglacial</i>	On top of the ice sheet or ice shelf.
<i>Surface ablation</i>	The process of melt or erosion of the surface (ice) layer
<i>Surface mass balance</i>	Mass balance of Antarctica. Antarctica loses mass by break up of ice shelves and by the melting of ice. Mass is gained by precipitation.

A.2. Datasets

Below, a table is presented which summarizes all datasets used in this study.

Table A.1: The datasets used

Dataset	Date retrieved	source/citation
REMA	March 2019	Howat et al. (2018)
RACMO	May 2020	van Wessem et al. (2018)
Landsat 8	October 2019	Courtesy of U.S. Geological Survey
Sentinel 2	October 2019	Copernicus Sentinel, processed by ESA
Depth, area and volume of meltwater features on the Nivlisen ice shelf	May 2020	Dell et al. (2020)

A.3. Additional figures

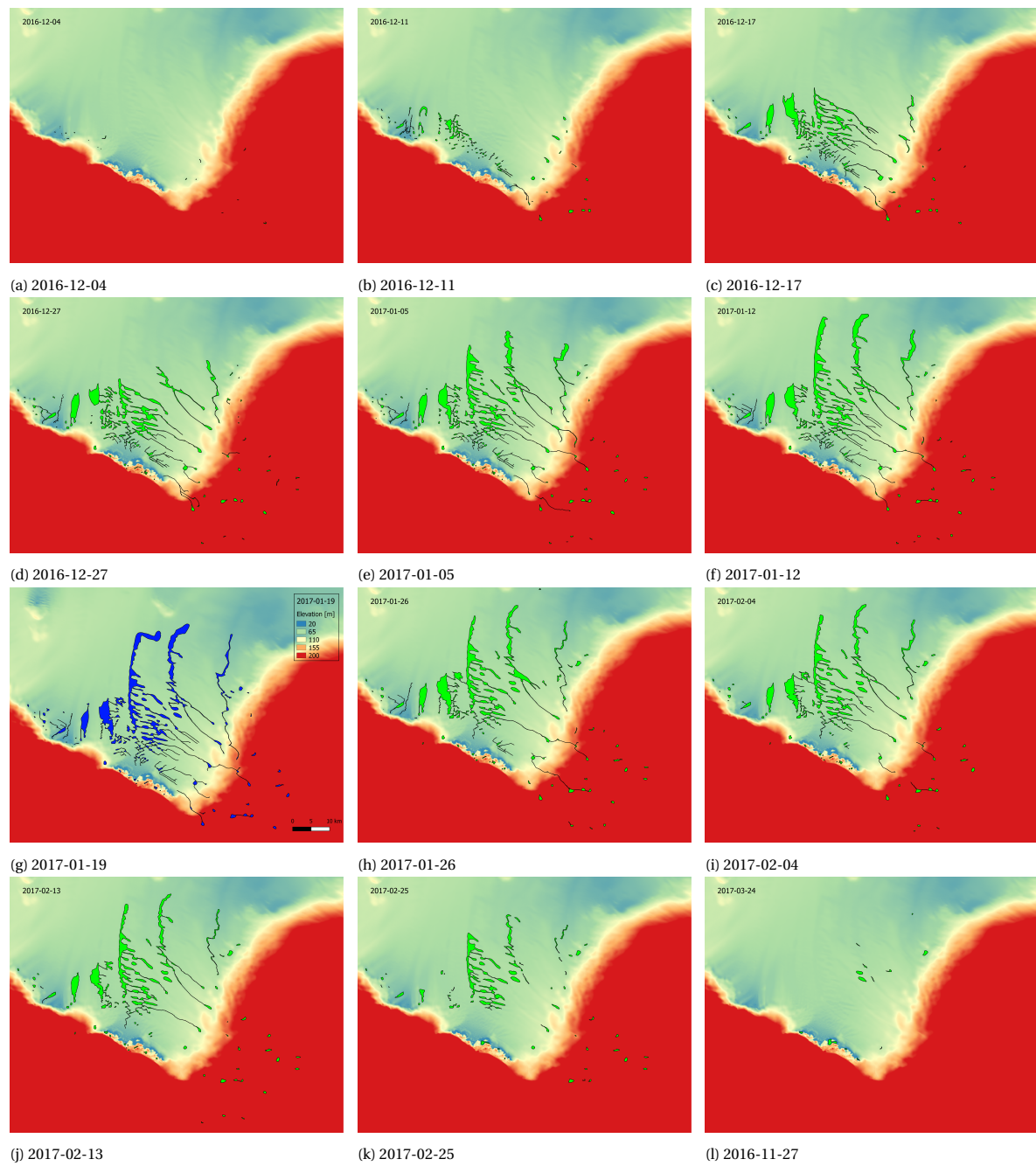


Figure A.1: The digitized water extent for each selected date for the 2016-2017 melting season on the Nivlisen ice shelf.

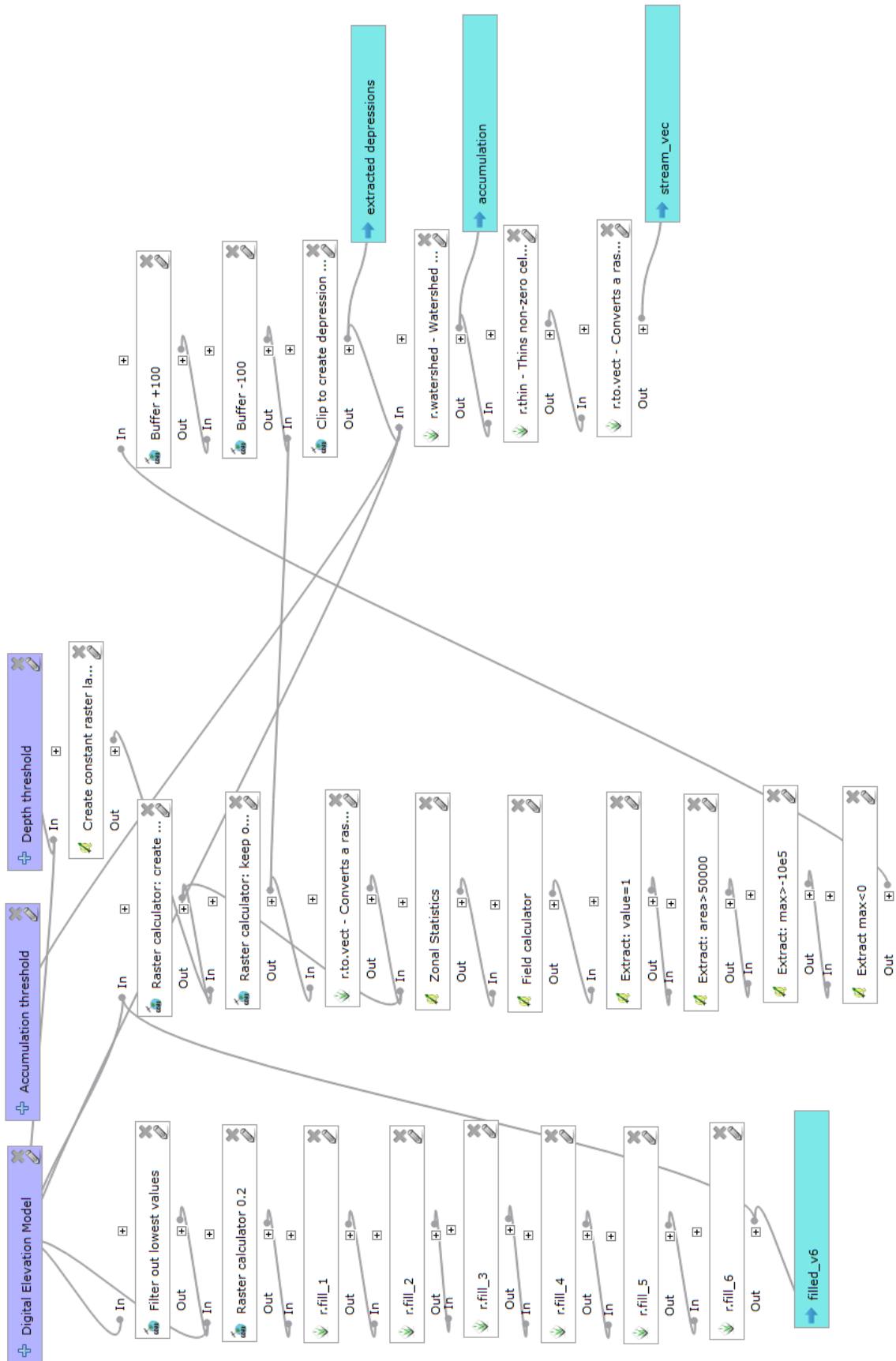


Figure A.2: Complete graphical modeller overview of the routing method developed for this study.